



# The glycoproteins EDIL3 and MFGE8 regulate vesicle - mediated eggshell calcification in a new model for avian biomineralisation

Lilian Stapane, Nathalie Le Roy, M. T. Hincke, Joël Gautron

## ► To cite this version:

Lilian Stapane, Nathalie Le Roy, M. T. Hincke, Joël Gautron. The glycoproteins EDIL3 and MFGE8 regulate vesicle - mediated eggshell calcification in a new model for avian biomineralisation. *Journal of Biological Chemistry*, 2019, 294 (40), pp.14526-14545. 10.1074/jbc.RA119.009799 . hal-02624751

**HAL Id: hal-02624751**

**<https://hal.inrae.fr/hal-02624751>**

Submitted on 26 May 2020

**HAL** is a multi-disciplinary open access archive for the deposit and dissemination of scientific research documents, whether they are published or not. The documents may come from teaching and research institutions in France or abroad, or from public or private research centers.

L'archive ouverte pluridisciplinaire **HAL**, est destinée au dépôt et à la diffusion de documents scientifiques de niveau recherche, publiés ou non, émanant des établissements d'enseignement et de recherche français ou étrangers, des laboratoires publics ou privés.

The glycoproteins EDIL3 and MFGE8 regulate vesicle - mediated eggshell calcification in a new model for avian biomineralisation

Lilian Stapane<sup>1</sup>, Nathalie Le Roy<sup>1</sup>, Maxwell T. Hincke<sup>2</sup>, Joël Gautron<sup>1\*</sup>

From <sup>1</sup>BOA, INRA, Université de Tours, 37380 Nouzilly, France; <sup>2</sup>Department of Innovation in Medical education, Department of Cellular and Molecular Medicine, University of Ottawa, Ottawa, K1H 8M5, Canada

Running title: *EDIL3/MFGE8 in avian shell calcification*

\*To whom correspondence should be addressed: BOA, INRA, Université de Tours, 37380 Nouzilly, France; [joel.gautron@inra.fr](mailto:joel.gautron@inra.fr); Tel. +33 2 47 42 75 40.

**Keywords:** biomineralisation, avian eggshell, EGF-like repeats and discoidin-like domains 3 (EDIL3), milk fat globule-EGF factor 8 (MFGE8), extracellular vesicles, protein evolution, vesicular transport, uterine fluid, glycoprotein

## ABSTRACT

The avian eggshell is a critical physical barrier, which permits extra-uterine development of the embryo. Its formation involves the fastest known biomineralisation process in vertebrates. The eggshell consists of proteins and proteoglycans that interact with the mineral phase to impart its specific microstructure and mechanical properties. In this study, we investigated the role of EGF-like repeats and discoidin-like domains 3 (EDIL3) and milk fat globule-EGF factor 8 (MFGE8), two glycoproteins that are consistently detected in eggshell proteomes. We verified their common evolutionary history and identified the timing of the duplication event giving rise to these two distinct proteins. *Edil3/mfge8* chromosomal locations revealed a nested syntenous relationship with other genes (*hapln1/hapln3* and *vcan/acan*) that are also involved in vertebrate calcification. EDIL3 and MFGE8 proteins possess epidermal growth factor-like (EGF-like) and coagulation factor 5/8 (F5/8C) domains, and their 3D structures predicted that they bind calcium and extracellular vesicles. In chicken, we confirmed the presence of EDIL3 and MFGE8 proteins in eggshell, uterine fluid and uterus. We observed that only *edil3* is overexpressed in tissues in which eggshell mineralisation takes place and that this overexpression occurs only at the onset of shell calcification. We therefore propose a model in which EDIL3 and, to a lesser extent, MFGE8 proteins guide vesicles containing amorphous calcium carbonate (ACC) to the mineralisation site. This model was supported

by the observation that extracellular vesicles (EV) accumulate in uterine fluid during eggshell calcification and that they contain high levels of calcium, carbon and oxygen that correspond to calcium carbonate.

The avian eggshell is a physical barrier against mechanical and microbial stresses that allows extra-uterine development of the embryo in a closed chamber. The eggshell consists of 95% calcium carbonate (CaCO<sub>3</sub>, calcite), 3.5 % organic matrix (OM; proteins, polysaccharides and proteoglycans) and 1.5 % water (1,2). This biomineral is composed of five layers: inner and outer eggshell membranes, two contiguous calcified layers (mammillary knobs and palisades) and the cuticle (3). Shell formation is extracellular and is the fastest biomineralisation process in vertebrates (4). Egg formation occurs in the hen reproductive tract (1,5). In chickens, the forming egg reaches the red isthmus (RI) at 4.5 h post-ovulation (p.o.), where shell biomineralisation is initiated on organic cores. The egg then enters the uterus (Ut), where it will remain for 18-19 h during shell calcification. Calcium carbonate is initially deposited as an amorphous phase (ACC), which progressively transforms into calcite (6).

During its formation, the shell is bathed in a uterine fluid (UF) secreted by uterine cells that contains the organic and mineral precursors necessary for shell calcification (7,8). Matrix proteins stabilise ACC, promote crystal nucleation, select the calcite polymorph and regulate the evolution of crystal size and morphology (4,7,9,10). These matrix-mineral

interactions determine the orientation of calcite crystals, which results in the complex ultrastructure of the eggshell, its texture and consequently its mechanical properties. Over the last couple of decades, numerous studies have defined the chicken eggshell matrix proteome (11-18). Currently, the entire dataset of reported proteins contains around 900 non-redundant proteins for the chicken eggshell and more than 600 for the UF (19,20). Amongst them, EDIL3 (EGF-like repeats and discoidin I-like domains 3) and MFGE8 (Milk fat globule-EGF factor 8), are reported in the majority of transcriptomics and proteomics studies associated with chicken eggshell biomineralisation (11,13-18,21,22). These two proteins were also identified in other avian eggshell proteomes (quail, turkey and guinea fowl) (23-25).

MFGE8 and EDIL3 are two secreted glycoproteins that have been well described in mammals and exhibit sequence similarity to each other. In avian eggshell, it was suggested that both EDIL3 and MFGE8 could bind  $\text{Ca}^{2+}$ , due to an EGF-like calcium-binding domain, and could favour crystal nucleation or change crystal morphology by selective interaction with calcium ion-rich crystallographic faces (19,21).

Nevertheless, the function of EDIL3 and MFGE8 is poorly understood. In this study, we have used bioinformatics tools to decipher the common evolutionary history of *edil3* and *mfge8* genes. We also explored the role of EDIL3 and MFGE8 in chicken eggshell mineralisation by predicting their molecular features, quantifying their gene expression and measuring protein levels in tissues involved in eggshell formation. Our study suggests that EDIL3 and MFGE8 would bind to vesicles and calcium carbonate to guide vesicular transport providing mineral cargo during avian eggshell biomineralisation.

## Results

### *The evolutionary history of EDIL3 and MFGE8: synteny and phylogenetic analysis*

EDIL3 and MFGE8 are two related proteins that share 54% identity and 69% similarity in *Gallus gallus* (EDIL3: XP\_424906.3; MFGE8: NP\_001264039.1; Table S1). They are encoded by two distinct genes, *edil3* and *mfge8*, which are localised on chromosome Z and chromosome 10, respectively. We compared their gene loci in

different vertebrate classes (fishes, amphibians, reptiles, birds and mammals; Fig. 1). *Edil3* and *mfge8* were observed to be nested in syntenous clusters containing *hapln1* (hyaluronan and proteoglycan link protein 1) and *vcn* (versican) adjacent to *edil3*, and *hapln3* (hyaluronan and proteoglycan link protein 3) and *acan* (aggrecan) adjacent to *mfge8* (Fig. 1). HAPLN1 and HAPLN3 belong to hyaluronan and proteoglycan link protein family and VCAN and ACAN belong to the lectican family. In chicken, HAPLN1 is related to HAPLN3 with 48% identity / 66% similarity for conservative substitutions, while VCAN and ACAN displayed 18% identity / 27% similarity (Table S1). The direction of *mfge8* gene cluster transcription is unchanged from Chondrichthyes (*Callorhinchus milii*) to Mammalia (*Homo sapiens*) (Fig. 1). This observation is also true for the *edil3* cluster during vertebrate evolution (Fig. 1). Therefore, the *edil3* and *mfge8* clusters are highly conserved in Gnathostoma. In birds, the *edil3* gene cluster is consistently observed on chromosome Z, while the *mfge8* cluster is found on a non-sexual chromosome (Table S2). These results confirm that the *edil3* and *mfge8* gene loci contain paralogous genes resulting from a duplication event.

In order to determine the timing of divergence between these two genes, we performed phylogenetic tree analysis of the protein sequences to investigate the evolutionary history of EDIL3 and MFGE8 in metazoans (Fig. 2). We first investigated the presence of the two proteins in eukaryotes. Blast analysis revealed that EDIL3 and / or MFGE8 were absent from protozoans to sponges. Consequently, the phylogenetic reconstruction was performed with EDIL3 / MFGE8 protein sequences from eumetazoan species (Fig. 2). The NCBI database contains a large number of EDIL3 / MFGE8 orthologues. To perform this analysis, we loaded 34 EDIL3 / MFGE8 sequences from 19 different species representing different taxa. These sequences belong to non-vertebrates (1 cnidarian, 1 platyhelminthe, 2 molluscs, 1 arthropod, 1 echinoderm and 1 cephalochordate) and vertebrates (2 fishes, 1 amphibian, 3 reptiles, 3 birds and 3 mammals; Table S3). MFGE8 sequences were often annotated as lactadherin in various databases (Table S3). For consistency during our analysis, all lactadherin sequences were renamed MFGE8 (Fig. 2). Sequences were aligned using clustalΩ multiple alignment. A

phylogenetic tree was constructed using Maximum Likelihood and Bayesian inference methods, which both conducted to similar tree topology and Maximum Likelihood result was displayed (Fig. 2). According to the topology of the tree, with coral *Acropora digitifera* EDIL3 protein as a rooted sequence, two distinct groups emerged within the phylogenetic tree. The first one contained non-vertebrate EDIL3 / MFGE8 sequences and the second one contained vertebrate EDIL3 / MFGE8 sequences. The latter group had a cephalochordate MFGE8 sequence as a root and is then divided into two clusters: vertebrate EDIL3 and vertebrate MFGE8 sequences respectively. Inside both clusters, we noticed that species were also grouped according to their class (actinopterygii, amphibian, reptiles, aves and mammals).

In Figure 2, the number of substitutions by site indicated that EDIL3 had undergone fewer changes during vertebrate evolution compared to MFGE8. Indeed, MFGE8 branches were longer than EDIL3 branches and the EDIL3 cluster bootstrap value (node value: 98) was higher than the value for the MFGE8 cluster (node value: 56). This result indicated that vertebrate sequences of MFGE8 were more divergent from each other than within the EDIL3 sequences. In non-vertebrates, EDIL3 and MFGE8 sequences did not form two distinct clusters. Moreover, we did not consistently observe both EDIL3 and MFGE8 protein sequences; in several non-vertebrates species only one sequence is present. These are mostly annotated as lactadherin-like (Table S3). The presence of both genes in the same non-vertebrate species, and their proximity in the tree, suggested that another duplication event affecting the ancestral *edil3/mfge8*-like gene appeared in the non-vertebrate lineages, as observed for the coral *Acropora digitifera*, the cephalochordate *Branchiostoma belcheri* and the sea urchin *Strongylocentrotus purpuratus*. We also observed during course of vertebrate evolution a distinction between *edil3* and *mfge8* emerging around 480 million years ago (MYA), which led to further diversification / divergence of their sequences and giving rise to vertebrate *edil3* and *mfge8*. This event occurred after the split of non-vertebrate / vertebrate lineages and before the split between fishes / amphibian phyla. Therefore, the *edil3 / mfge8* divergence appeared between 684 and 473 million years ago.

A comparison of protein domains was performed throughout eumetazoan evolution (Fig. 2). In non-vertebrates, only EDIL3 of the coral *Acropora digitifera* possesses EGF-like domains whereas this domain was present in all EDIL3 / MFGE8 vertebrate species. The most primitive vertebrate of the study (*Callorhinchus milii*) possessed three EGF-like domains in MFGE8, and only two in its EDIL3. With the notable exception of fishes, all EDIL3 vertebrate sequences contain three EGF-like domains. Three EGF-like domains are also present in non-mammalian MFGE8 sequences, whereas two and one are present in non-primate mammals and primates, respectively. A Ca<sup>2+</sup>-binding motif is also present in *Acropora digitifera* EDIL3 and in all other sequences except in fishes EDIL3, mammalian MFGE8 and non-vertebrates. An RGD motif (integrin, ITG-binding) was also detected in EGF-like domains of all vertebrate MFGE8s and EDIL3s. In non-vertebrates, this motif is observed in F5/8C domains, when present. This latter domain was observed in all vertebrate and non-vertebrate sequences. A double RGD motif was also detected in three non-vertebrate sequences and in *Gallus gallus* EDIL3. However, the vertebrate RGD sequences are found in the EGF-like domains, whereas the invertebrate RGDs are located within the F5/8C regions.

#### **Edil3 and mfge8 expression in Gallus gallus tissues at various stages of shell mineralisation**

We investigated the level of expression of both genes in oviduct tissues involved in egg white and eggshell formation (Fig. 3A). These are the magnum (Ma) where egg white proteins are synthesised and the white isthmus (WI) where the shell membranes are formed. In addition, the red isthmus (RI) and uterus (Ut) are involved in the onset and development of shell mineralisation, respectively. Gene expression in these oviduct segments was compared to samples from mid-shaft tibial bone (B) (mineralised tissue), duodenum (D) (high calcium intake), kidney (K) (involved in ion exchange) and finally liver (L) as an important tissue of general metabolism. Levels of expression were measured in tissues harvested during the onset of the rapid growth phase of shell mineralisation (10 h p.o., except for B collected at 18 h p.o. when shell mineralisation and bone demineralisation are completed).

*Edil3* expression was low in D, L, Ma, B and K and not significantly different from



background levels (Fig. 3A). *Edil3* was significantly expressed in tissues involved in shell formation in contrast to the five other tissues. They were, however, not significantly different from each other. RI / B and Ut / B expression ratios were 58.6 and 39.2, respectively, and 846.9 and 566.9, respectively, for RI / K and Ut / K ratios. *Mfge8* was expressed in all tissues (Fig. 3A). Liver exhibited the highest level of *mfge8* expression followed by RI. *Mfge8* expression levels were significantly different in these two tissues, which were both significantly different from the six other tissues. Ratios of RI expression were 73, 18.3, 4.1, 2.5 and 2.6 with Ma, D, B, K and WI, respectively.

Levels of *edil3* and *mfge8* expression in oviduct regions that are active during eggshell mineralisation (Ut and RI) were measured at five key stages of shell calcification. *Edil3* was expressed at all stages in Ut and RI, and was significantly higher in Ut for stages 6 h and 7 h p.o. compared to 16 h p.o. (Fig. 3B, C), when ACC is massively deposited with the first aggregates of calcite forming around mammillary knobs. *Edil3* expression compared to 16 h p.o., exhibited a fold change of 5.6 and 4.9, at 6 h and 7 h p.o. respectively. In contrast, from 5 h to 16 h p.o., no significant difference was observed for *edil3* in RI and for *mfge8* in Ut and RI (Fig. 3B, C).

### ***EDIL3 and MFGE8 protein levels during eggshell formation***

The presence of EDIL3 and MFGE8 proteins was investigated in soluble eggshell matrix (SEM), uterine fluid (UF), uterus (Ut) and duodenum (D) (which is involved in ion transfer without mineralisation). Using anti-EDIL3 antibodies, a single immunoband was observed around 60-kDa (expected size 54-kDa) in SEM, Ut and to a lesser extent, in UF (Fig. 3D). No immunoreactive band was observed in D. MFGE8 exhibited an intense immunoreactive band in all tissue samples, including D (Fig. 3D) at 75-kDa (expected 53-kDa). The higher than predicted molecular mass observed for MFGE8 could be due to post-translational modification such as glycosylation, which has been reported for this protein (26,27). These results are in accordance with expression measurements, and confirmed that EDIL3 is specific to the oviduct tissue involved in shell mineralisation, whereas MFGE8 is present in a variety of tissues or

organs, including those responsible for eggshell calcification (Fig. 3).

### ***Characterisation of Gallus gallus EDIL3 and MFGE8 functional domains***

We explored gene and protein sequences of EDIL3 and MFGE8 using bioinformatics tools. *Gallus gallus edil3* is made of 11 exons and is located on sex chromosome Z (Fig. 4). Its transcription leads to two different transcripts of 5544 and 1973 nucleotides coding for 480 and 470 amino acid proteins, respectively (NCBI). Differences in transcript size are the consequence of a 30-nucleotide deletion in exon 3 and alternative splicing of exon 11. This latter alternative splicing does not affect the translated protein because it modifies the 3'-UTR region in the mRNA. Stop codons are located at positions 1657-1659 and 1687-1689 in the short and long mRNA variants, respectively. The 30-nucleotide in-frame deletion of exon 3 resulted in a loss of 10 amino acids between two EGF-like domains. The *Gallus gallus mfge8* gene is located on chromosome 10 and is made of 10 exons (Fig. 4). As is the case for *edil3*, *mfge8* also exhibited two transcripts of 2588 and 2570 bases, which encode proteins of 474 and 468 amino acids, respectively (NCBI). The shorter transcript is the result of an 18-nucleotide deletion at the onset of the last exon, which induces a loss of six amino acids between two F5/8C domains of the corresponding protein. The remaining sequence is not affected by this deletion.

EDIL3 and MFGE8 *Gallus gallus* proteins were aligned with MEGA7 software, and protein domains were investigated using PROSITE (Fig. 5). Both proteins exhibited three EGF-like domains at the N-terminus (Fig. 5, protein 1 in Fig. 4). Residues 22-60 and 24-62 correspond to EDIL3 and MFGE8 EGF-like 1 domains, respectively. Other EGF-like domains were located at positions 74-117, 65-107 and 119-155, 109-145 for domains 2 and 3 of EDIL3 and MFGE8, respectively. EDIL3 EGF-like 1 and 2 domains possess an ITG-binding site (RGD motif in positions 22-24 and 96-98), while this motif was only present in the EGF-like 2 domain for MFGE8 (position 86-88). Both proteins also possess a Ca<sup>2+</sup>-binding motif in the EGF-like 3 domain. This motif was composed of about 40 residues with six cysteine residues that form three disulphide bonds with the following consensus pattern nxnnC-x(3,14)-

C-x(3,7)-CxxbxxxxxaxC-x(1,6)-C-x(8,13)-Cx. This  $\text{Ca}^{2+}$ -binding motif was found in positions 119-143 and 109-133 for EDIL3 and MFGE8 respectively. Alignments of *Gallus gallus* EDIL3 and MFGE8 EGF-like 3 domains with *Homo sapiens* coagulation factors IX/X EGF-like domains are represented on Figure S1A. The  $\text{Ca}^{2+}$  consensus sequence of human coagulation factors IX/X are depicted in Figure 5. The  $\text{Ca}^{2+}$ -binding motifs of EGF-like 3 domains translated from the longer transcripts of *Gallus gallus* EDIL3 (N119, N121, D136, Y141) and MFGE8 (N109, N111, D126, Y131) were highly conserved when compared to the EGF-like  $\text{Ca}^{2+}$ -binding consensus sequences of the human protein (D1, D3, D18, Y23; Figs. 5, S1A). However both Asp (D) of the human coagulation factors IX/X  $\text{Ca}^{2+}$ -binding motif were replaced by Asn (N, residue with a similar polar property to D) in each *Gallus gallus* protein. Cysteines were strictly conserved between both proteins at the  $\text{Ca}^{2+}$ -binding site.

We also observed two F5/8C domains in both EDIL3 and MFGE8 C-terminal regions (positions 158-314, 319-476 and 148-304, 315-472, respectively, Fig. 5). Finally, phosphatidylserine-binding (PS-binding) motifs have been reported in the mammalian sequences and we investigated the presence of this motif in both EDIL3 and MFGE8 from *Gallus gallus*. The following residues (K24, W26, F31, K45, Q76, R79, F81, R146) were described in *Mus musculus* protein as involved in PS-binding (28). The same residues were observed in positions 338, 340, 345, 359, 390, 393, 395 and 453 of the F5/8C 2 domains of *Gallus gallus* MFGE8, while EDIL3 shown identical and similar residues (R-FKQKFR) in positions 342, 349, 363, 394, 397, 399, 466 (Figs. 5, S1B). Trp (W) is not present in the EDIL3 sequence and conservative substitutions (K / R and R / K) are observed in positions 342 and 397, respectively. However, an absence of Trp at this position did not affect the function of the PS-binding site (28); consequently, these data suggest potential functional PS-binding activity for both *Gallus gallus* EDIL3 and MFGE8 proteins.

We performed computational predictions of secondary structure for chicken EDIL3 and MFGE8 using PSIPRED v3.3 and I-TASSER program server. Twenty-two  $\beta$ -sheets and two  $\alpha$ -helix were predicted for EDIL3, and 25  $\beta$ -sheets and two  $\alpha$ -helix for MFGE8 proteins, with good correspondence between

the 22  $\beta$ -sheets of EDIL3 and those in MFGE8. We also observed that EGF-like domains are made up of two  $\beta$ -sheets in each protein. The first F5/8C contains 11  $\beta$ -sheets in MFGE8 and nine in EDIL3, whereas the second is similar in both proteins with seven  $\beta$ -sheets.

The 3D structures of EDIL3 and MFGE8 were also predicted with I-TASSER program server (molecular homology modelling) and the spatial arrangement of amino acids involved in each binding function (ITG,  $\text{Ca}^{2+}$  and PS) was highlighted on the 3D structure models using PyMOL Molecular Graphics system (Fig. 6A, C). A close spatial proximity among residues was observed in accordance with their ability to interact with their substrates and consequently we predicted that these domains are functional. The conformation of the  $\text{Ca}^{2+}$ -binding domain was composed, as expected, of three disulphide bridges necessary to maintain the protein conformation for interaction with  $\text{Ca}^{2+}$  (Fig. 6A, C). The spatial arrangement of residues in the second F5/8C domains associated with the PS-binding motif in *Gallus gallus* are highlighted (Fig. 6 A, C). This motif involves 7 and 8 amino acids for EDIL3 and MFGE8, respectively. Residues are located in three different loops as observed for the mammalian sequences (Fig. 6 A, C, green balls). Only Q390 was observed in a  $\beta$ -sheet in the MFGE8 F5/8C 2 domain. Both EDIL3 and MFGE8 RGD motifs involved in ITG-binding of the second EGF-like domains were localised to a loop between two  $\beta$ -sheets (Fig. 6, orange balls). Structural modelling also indicates that the major difference between EDIL3 and MFGE8 is associated with the first EGF-like domain (Fig. 6), for which an additional specific RGD motif was observed in EDIL3. This additional RGD motif is not located in a loop between  $\beta$ -sheets.

## Discussion

EDIL3 and MFGE8 are two proteins widely detected in proteomic studies associated with chicken eggshell biomineralisation (11,13-18,21). In chicken these two proteins exhibited a high abundance in partially mineralised eggshell at the initiation of biomineralisation and consequently they are thought to be potential major actors in the calcification process (21).

MFGE8 and EDIL3 are homologous secreted glycoproteins that have been well described in mammals. The *mfge8* transcript

was first identified in mouse mammary epithelial cells (29). MFGE8 is known to participate in a wide variety of cellular interactions such as macrophage and apoptotic cells bridging, adhesion between sperm and the *zona pellucida* of the egg or exosome function (30-34). EDIL3 was first identified in mouse as an extracellular matrix protein involved in embryonic vascular development and demonstrating an angiogenic role (35-37). In mammals, EDIL3 is physiologically expressed in various tissues such as brain, intestine, heart and kidney (38). EDIL3 was also detected during cancer development and is expressed by primary tumours from breast and colon cancers (39). In breast cancer, EDIL3 was identified on extracellular vesicles (EV) promoting cellular invasion and was suggested to be a potential biomarker for monitoring this metastatic cancer (40). In developing chicken embryos, experiments have been performed on chorioallantoic membrane (CAM) using mammalian EDIL3 (DEL1). DEL1 was found to be involved in embryonic vascular remodeling, in mediating the breakdown of existing vascular bloods and inducing restructuring of the CAM vasculature (35). In contrast, a potent pro-angiogenic activity was reported for DEL1 in chicken CAM, which was mediated by integrin ( $\alpha\beta3$ ) activation *via* the RGD motif (36).

Our phylogenetic analysis demonstrated that vertebrate *edil3* and *mfge8* are derived from a duplication event of an ancestral common gene. The divergence point between these two paralogs was estimated to be about 480 MYA. Gene duplication processes are crucial to generate genes with novel or altered functions (41). The duplication events giving rise to *edil3* and *mfge8* in early vertebrates emerged prior to the appearance of the amniotic egg at the split between amphibians (uncalcified egg) and reptiles (calcified egg, Amniota) that occurred around 350 MYA (42,43). According to our study, the function of EDIL3 and MFGE8 was recruited to diverse biological processes, including eggshell calcification.

In non-primate mammals, two homologous domains of epidermal growth factor from drosophila NOTCH (EGF-like), at the N-terminus and one tandem of discoidin-like domains similar to those of coagulation factors V and VIII (F5/8C) at the C-terminus were described in MFGE8 (29,44). Our

evolutionary study confirmed the presence of these domains in mammals and also explored additional eumetazoan sequences used in this study. The F5/8C domains appear to be present in all species sequences indicating an origin of this domain in the common ancestor of eumetazoans. The number of F5/8C domains is variable in non-vertebrates (from 2 to 4) whereas it is constant in vertebrates, in which two F5/8C were reported. The PS-binding site of MFGE8 orthologs was previously described in cow (*Bos Taurus*) and mouse (*Mus musculus*) (28,45-48). The following residues (K24, W26, F31, K45, Q76, R79, F81 and R146) are major residues contributing to the interaction between the F5/8C 2 domain of MFGE8 and PS in mouse (28). Several studies reported the mechanism of mammalian MFGE8 F5/8C binding to PS (47,49). PS-binding allows MFGE8 to complex with vesicles or cell membranes through their second F5/8C domain to perform physiological functions such as cellular interactions and exosome transport (30,31,33). Thus, mammalian MFGE8 binds to PS-containing vesicles in a two-step mechanism that explains the strong enrichment of MFGE8 in exosomes from dendritic cells (30,47). We identified this motif in the *Gallus gallus* EDIL3 / MFGE8 sequences suggesting that chicken EDIL3 and MFGE8 proteins can also bind to membrane phospholipids.

EGF-like domains are present in all vertebrates but absent in non-vertebrates with the notable exception of EDIL3 of the Cnidaria *Acropora digitifera*, which is the most primitive eumetazoan species used in the present study. In vertebrates, three EGF-like domains were present, except for EDIL3 in fishes (two domains) and MFGE8 in mammals (two and one domains in non-primates and primate, respectively). This result confirms previous findings on mammalian MFGE8 (27,50). The highest conserved EGF-like domain in vertebrate species includes an RGD motif (arginine, glycine and aspartic acid) in both MFGE8 and EDIL3 proteins. This motif displays a strong affinity for  $\alpha\beta3$  /  $\alpha\beta5$  integrins (ITG), which are expressed at the cell surface and widely present in vertebrates, underlying its major role in cellular interactions (30,31,33,34). It is present in the second and third EGF-like domains in vertebrates. In non-vertebrates, the RGD site is found in the F5/8C domain of protostomian species (arthropods, molluscs and trematodes) and is completely



absent in others (Fig. 5). These results suggest the independent acquisition of RGD motif in protostomians and in vertebrates. We also predict a  $\text{Ca}^{2+}$ -binding motif in the third EGF-like domain of EDIL3 and MFGE8 in the majority of the vertebrates sequences analysed. However, this motif was not observed in mammalian MFGE8 or in EDIL3 of fishes selected for this study. The  $\text{Ca}^{2+}$ -binding motif was therefore lost in MFGE8 at the split of oviparous / viviparous vertebrates. Interestingly, MFGE8 was reported as the major component of the milk fat globule membrane, which is a calcium rich milieu (51). In non-vertebrate species,  $\text{Ca}^{2+}$ -binding sites were only found in the EDIL3 sequence of the staghorn coral (*Acropora digitifera*), which precipitates a calcium carbonate exoskeleton. However, we did not identify  $\text{Ca}^{2+}$ -binding motifs in protein sequences of the purple sea urchin (*Strongylocentrotus purpuratus*) or the eastern oyster (*Crassostrea virginica*), which also mineralise a  $\text{CaCO}_3$  skeleton. The cephalochordate *Branchiostoma belcheri*, which is a "fish-like" species without a calcareous skeleton, did not exhibit this motif.

The question of the role(s) of these two proteins in avian eggshell formation is the main focus of this study. EDIL3 and MFGE8 were initially proposed to be important molecular actors in chicken eggshell mineralisation (21). They were quantified at the four key steps of shell mineralisation and classified according to their abundance (21). Amongst the 216 eggshell proteins quantified in this study, EDIL3 abundance was amongst the top ten proteins at the two stages corresponding to the transformation of ACC into calcite crystals. The abundance of MFGE8 was intermediate in the shell, whatever the stage of shell mineralisation (21). A comparative study revealed that MFGE8 is overabundant in the proteome of strong eggshells compared to weaker shells (15). In addition to their detection in numerous investigations of the chicken eggshell proteome, both proteins were identified in other avian eggshell proteomes (quail, turkey and guinea fowl) (23-25). The experiments performed in this study support our hypothesis that EDIL3 plays a key role during eggshell formation. *Edil3* was overexpressed in the oviduct regions where eggshell formation takes place (WI, RI and Ut), and EDIL3 protein was present in SEM, UF and Ut. We also compared *edil3* expression levels with those of other

uterine genes during eggshell calcification. We have previously observed by RNA-Seq that the *edil3* Counting Per Million (CPM) value was about 3 times higher than the median CPM value of genes coding for eggshell matrix proteins (52,53). The median emPAI of proteins quantified in the shell proteome is 5.92, while the maximum emPAI was obtained for Lysozyme with a value of 13537. The second most abundant protein was Ovocleidin-116 (OC-116, MEPE) with an emPAI value of 7168. EDIL3 exhibited a value of 3523 and was the sixth most abundant eggshell protein. MFGE8 was the 34<sup>th</sup> most abundant protein with an emPAI value of 37.5. The role of MFGE8 in chicken eggshell biomineralisation is not so clear. Indeed, *mfge8* was significantly overexpressed in RI where shell mineralisation is initiated, but its expression is not specific to the oviduct segment where shell mineralisation occurs; moreover, it is ubiquitous in all tested tissues, with the highest levels in liver. Nevertheless, its levels in uterus determined by RNA-Seq were about 2 times higher than the median CPM value for genes encoding matrix proteins (52,53).

In mammals, MFGE8 was reported to be involved in spermatozoid-egg *zona pellucida*-binding (54). In bird eggs, the vitelline membranes that surround the yolk contain *zona pellucida* proteins that originate from the liver (55). Therefore, MFGE8 could play a role in spermatozoid adhesion. Western blotting confirmed the presence of MFGE8 protein in shell, uterine fluid and uterus, but also in duodenum. In birds, the duodenum is not involved in shell calcification but plays a key role in the uptake of dietary calcium to provide the ions necessary for bone and eggshell formation (56).

Our exploration of *edil3* and *mfge8* chromosomal arrangements throughout vertebrate evolution highlighted a strongly conserved synteny for both genes (Fig. 1). In avian species, we observed that *edil3* and *mfge8* are localised on chromosome Z and on a non-sexual chromosome, respectively. Interestingly, quantitative trait loci (QTL) affecting chicken eggshell strength are present on the Z chromosome (57,58). Moreover, we observed that the adjacent genes at the *edil3* and *mfge8* loci are *hapln1* / *vcan* and *hapln3* / *acan*, respectively. HAPLN3 is one of the most abundant proteins in the chicken eggshell and HAPLN1 was identified in the eggshell



membranes of fertilised eggs (21,59). Proteoglycans play an important role in eggshell biomineralisation; for example, the dermatan sulfate proteoglycan ovocleidin-116 (MEPE) is abundant in eggshells (21,60-63). Proteoglycan macromolecules combine a protein core with a negatively charged complex polysaccharide, and strongly interact with calcium (64). In mammals, HAPLN1, ACAN and VCAN are cartilage matrix proteins and they participate in multi-molecular aggregates (65-67).

Numerous studies on mammals revealed the participation of vesicles in bone and cartilage mineralisation (68-73). A non-crystalline calcium phosphate phase was shown within intracellular vesicles of bone-lining cells (74). Membrane-bound mineral particles have been identified in osteoblasts (75), and numerous vesicles containing calcium phosphate are also present in the circulatory system or in the extracellular space adjacent to osteoblasts during embryonic chicken long-bone development (76). Additionally, MFGE8 is an abundant protein in mineralising vesicles from chicken embryonic femurs, and was also present with EDIL3 in mammalian cartilage vesicles (77-79). Furthermore, HAPLN1, ACAN and VCAN were also identified in these vesicles (77,78,80). Recently, an RNA-Seq study reported that several vesicular genes are highly expressed in hen uterus (52). For example, *pdc6ip* and *sdcbp* encode proteins (PDCD6IP and Syntenin-1) found in matrix vesicles isolated from bone or cartilage (79). In addition, electron microscopy studies of hen utero-vaginal junction detected a large number of vesicles released into the lumen (81). Spherical voids can be visualised by scanning electron microscopy in the calcified eggshell (82,83), which we hypothesise are the remnants of mineralisation-associated matrix vesicles. Spherical structures ( $\approx 300$  nm) are observed within the organic matrix of decalcified eggshell (82); they are observed throughout the entire palisade layer and upper mammillary knobs, and are immunoreactive for the eggshell proteoglycan ovocleidin-116 (84-87).

We hypothesise that extracellular vesicles are involved in eggshell formation. Chicken eggshell biomineralisation requires ACC to supply ions for rapid mineralisation (88,89). Indeed, ACC was reported as an important highly reactive translational phase for formation of sea urchin spines or molluscan

shells (89-91). In chicken eggshell, ACC is first massively deposited on the entire surface of the shell membranes, and then accumulates at specific nucleation sites to supply ions to form calcite (6). ACC is highly unstable under physiological conditions and consequently the vesicles observed in eggshell could stabilise and transport ACC during mineralisation. *In vitro* studies have shown that liposome vesicles can stabilise ACC and prevent its premature crystallisation (92). Indeed, uterine fluid is a supersaturated solution (93); therefore, transport of ACC via vesicles through the uterine fluid would avoid ectopic calcification, as proposed for bone mineralisation by calcium phosphate (75). We also reported in this study that *Gallus gallus* EDIL3 and MFGE8 have  $\text{Ca}^{2+}$ -binding and PS-binding sites. PS-binding would allow their attachment to vesicle membranes and the  $\text{Ca}^{2+}$ -binding domain could interact with the mineral phase. We therefore propose a model in which EDIL3 and MFGE8 would guide vesicles containing ACC cargo to the site of mineralisation (Fig. 7). This hypothesis is supported by the description in dendritic cells exosomes of MFGE8 targeting effector cells ITG as a guiding protein (30). The presence of vesicles in  $\text{CaCO}_3$  mineralisation has been described in sea urchin embryos (94). In the present study, EDIL3 and MFGE8 were observed in Ut and UF and would be present in vesicles originating from uterine epithelial cells, transiting through the UF and targeting  $\text{Ca}^{2+}$  to the mineralisation site to deliver the mineral precursor (Fig. 7). We used transmission electronic microscopy (TEM) to analyse uterine fluid and confirmed the presence of extracellular vesicles (EV) in the 100-300 nm size range in this milieu (Fig. 8). We also performed energy dispersive X-ray spectroscopy (EDS) on vesicles to detect elements present in vesicles (Fig.9). Several mapping measurements were obtained across a vesicle (Fig. 9B) or mapped point by point at different sites where vesicles were present or absent (Fig. 9C). The spectra showed that calcium, carbon and oxygen were present in vesicles in agreement with calcium carbonate. However, phosphorus and chlorine, representing alternative counterions for calcium (phosphate and chloride), were not detected at these levels. This result is robust evidence for calcium carbonate inside UF vesicles and highlights their contribution to the transport of calcium necessary for calcification.

Moreover, we confirmed that both proteins are incorporated into the shell matrix during mineralisation. Additionally, our results highlighted *edil3* and *mfge8* expression throughout eggshell formation and notably at the early stages for *edil3* when ACC deposition is massive (6). This scenario would take place during the entire process of shell formation, as ACC is required at the mineralisation front (6).

We surveyed previous chicken eggshell and uterine fluid proteomic studies (11,15,19,21) to identify additional proteins potentially involved in our proposed vesicular transport model (Table 1). Annexins (ANX) should be involved in vesicular transport as shown *in vitro* for cartilage or bone (95-97). Indeed, ANXs can act as a  $\text{Ca}^{2+}$  channel in vesicle membranes (Fig. 7) (98-100). ANXA1, ANXA2, ANXA5 and ANXA8 are detected in the chicken eggshell and their encoding genes are highly expressed in uterine cells (11,15,21,52). ANXA2 is also identified in other bird eggshell proteomes such as duck, quail, turkey and guinea fowl, suggesting a common role in shell biomineralisation (25,101). Eggshell  $\text{CaCO}_3$  requires bicarbonate ions in addition to calcium to form ACC. This role of  $\text{HCO}_3^-$  supplier inside the vesicles could be ensured by carbonic anhydrases (CAs), which transform soluble  $\text{CO}_2$  into bicarbonate ions (Fig. 7). Indeed, the UF has a high partial pressure of  $\text{CO}_2$  (100 mm Hg) which is 2-fold elevated compared to plasma (93,102). Amongst the members of the CA family, CA4 is present in the eggshell proteome of chicken, duck, quail, turkey and guinea fowl (25,101). CA4 is a GPI-anchored protein that is attached to plasma membrane, and consequently we predict that it is present in the extracellular vesicles. Ovocleidin-17 (OC-17), ovalbumin (OVAL) and lysozyme (LYZ) are three chicken eggshell proteins described as ACC stabilisers (103-105). Finally, we used the Vesiclepedia database (106) to explore vesicular markers amongst chicken shell proteins already identified (Table 1). We found seven groups of EV marker proteins according to their function: chaperone proteins (HSPs), biogenesis factors (PDCD6IP, EZR and Syntenin-1), cell adhesion (FN1), intracellular trafficking proteins (Rab10), membrane organiser (CD9), signalling proteins (YWHAZ, YWHAЕ) and other cargo (ALB, GSN, VCP...). Moreover, EZR, FN1, GSN, HSPA5, PDCD6IP and Syntenin-1 are present in several avian eggshell proteomes

(chicken, duck, quail, turkey) (101). Their presence in several proteomes highlighted their central role in the shell mineralisation process. These proteins could play functional roles in the vesicular transport model proposed herein.

In the present study, we used a bioinformatics approach to delineate the evolutionary history of *edil3* / *mfge8* in Eumetazoa, and suggest that EDIL3 and MFGE8 proteins in vertebrates are derived from a duplication event, as supported by observed synteny in these and adjacent genes. Our gene expression and immunochemistry results allow us to propose a coherent model for EDIL3 and MFGE8 function in vesicles that deliver stabilised ACC for shell mineralisation. This scenario involves the vesicular transport of both  $\text{Ca}^{2+}$  and  $\text{HCO}_3^-$  in the uterine fluid and predicts the involvement of additional vesicular genes, such as annexins. We confirmed the presence of extracellular vesicles in the uterine fluid and detected the elements of calcium, carbon and oxygen (calcium carbonate) within them.

## Experimental procedures

### Ethical statement animal handling and housing

Present experiments, including animal handling protocols, were performed in accordance with European Communities Council Directives concerning the practice for the care and use of animals for scientific purposes and the French ministry of Agriculture on animal experimentation under the supervision of authorised scientists (authorisation #7323, delivered by the “Direction Départementale de la Protection des Populations d’Indre et Loire-France”, DDPP). Experimental unit (UE-PEAT 1295), where the birds were housed, has an agreement to rear birds and to euthanise experimental animals (decree No C31-175-1 of August 28<sup>th</sup> 2012 delivered by the “Préfecture d’ Indre et Loire”). The experimental protocol was accepted by the CEEA VdL ethical committee (French national ethics committee for animal experimentation n°19) and the French ministry under #16099-015902.

### Uterine fluid, egg and tissue collections

Thirty-six mature brown laying hens (ISA-Hendrix, 40 and 90 weeks old) were placed in individual furnished cages with automatic devices for recording of the oviposition times. Animals were fed *ad libitum* (layer mash) using a commercial feed for layers.

Laying hens were subjected to a cycle of 14 h of light / 10 h of darkness. Following collection and opening of eggs, the eggshells were thoroughly washed with water, air dried and stored at -20°C.

Uterine fluids (UF) were collected as described previously (7). Briefly, egg expulsion was induced by an intravenous injection of 50 µg Dinolytic® prostaglandin-F2α (Zoetis, Malakoff, France) at 7-9 and 16 h p.o., which correspond to the initiation and active phase of shell mineralisation. Immediately after egg expulsion, UF were collected by gravity in a tube placed at the entrance of the everted vagina. UF were directly frozen in liquid nitrogen in the form of beads or diluted into phosphate buffer saline (PBS). UF samples were stored at -20°C until use. An additional UF aliquot was also diluted 5x for SDS-PAGE into Laemmli sample buffer, for a final composition of 0.0415 M Tris-HCl, pH 6.8, 1% SDS, 10% glycerol, 1.66% β-mercaptoethanol and 0.01% bromophenol blue.

Tissues were collected from thirty 40 week-old and six 90 week-old laying hens. Animals were euthanised with Dolethal® (Vetoquinol, Magny-vernois, France) at the initial phase of eggshell mineralisation (5, 6 and 7 h p.o., when the nucleation sites appear and early mineralisation starts), at the beginning of the active calcification phase (10 h p.o.) or during the linear growth phase of rapid calcification (16 h p.o.). Various tissues (Duodenum, D; Kidney, K; Liver, L) and oviduct regions (Magnum, Ma; White isthmus, WI; Red isthmus, RI and Uterus, Ut) were collected from birds at each stage of shell calcification. Mid-shaft tibial bone (B) from 90 week old hens (18 h p.o., at the end of bone resorption) were also harvested. Tissues were directly immersed in liquid nitrogen and were kept at -80 °C.

#### ***Soluble eggshell matrix and tissues protein extraction***

Eggshell matrix proteins from eggs were extracted as previously detailed (107). Briefly, eggshell pieces with eggshell membranes were immersed in 154 mM NaCl solution containing protease inhibitors (2.5 mM benzamidine-HCl, 50 mM ε-amino-n-caproic acid, 0.5 mM N-ethylmaleimide, and 1 mM phenylmethylsulfonyl fluoride), and ground into a fine powder. Eggshell powders were fully demineralised by immersion in 20% acetic acid

with overnight stirring at 4 °C. The resulting suspensions were dialysed (cut off 3,500 Da) against demineralised water during 24 h at 4 °C and lyophilised. Samples were then incubated overnight at 4 °C in 4 M guanidine-HCl, 5 mM benzamidine-HCl, 0.1 M ε-amino-n-caproic acid, 10 mM EDTA, 50 mM sodium acetate, and 1 mM phenylmethylsulfonyl fluoride. Samples were then dialysed (cut off 3,500 Da) against 0.5 M sodium acetate pH 7.4 solution during 24 h at 4 °C and then centrifuged for 10 min at 2,000 g at 4 °C. The resulting supernatants were stored at -20 °C.

Harvested tissues were homogenised with ULTRA-TURRAX® (IKA, Staufen, Germany) in Tris buffered saline (TBS; 50 mM Tris-HCl, 77 mM NaCl, pH 7.4, and protease inhibitors), for 0.2 g/mL of tissue in each extraction solution. Samples were then centrifuged for 30 min at 10,000 g and supernatants were stored at -20 °C.

#### ***Electrophoresis and Western blot analysis***

Protein concentrations were determined in various samples (Soluble Eggshell Matrix, SEM; Uterus 10 h, Ut; Uterine fluid 9 h, UF and Duodenum 10 h, D), using BioRad DC Protein Assay kit II (BioRad, Marnes-la Coquette, France) in accordance with manufacturer's instructions and using bovine serum albumin as a standard. Fifteen micrograms of each sample (SEM, UF, Ut and D) were diluted into Laemmli sample buffer (5:1) as previously described and boiled for 5 min. Protein samples were then separated on 12% polyacrylamide gels (Mini-Protean II electrophoresis cell, BioRad, Marnes-la-Coquette, France) and transferred onto 0.2 µm nitrocellulose blotting membrane (GE Healthcare, Little Chalfont, England) for Western blot analysis. Membranes were washed 5 min in TBS (50 mM Tris-HCl, 150 mM NaCl, pH 7.4) and incubated for 2 h with the Odyssey® blocking buffer (LI-COR, Bad Homburg, Germany) in TBS (1:1). Membranes were then incubated for 3 h in the blocking solution, containing 0.1% Tween-20, with rabbit polyclonal anti-EDIL3 (1: 1,000; SAB2105802, Sigma-Aldrich, Saint-Quentin Fallavier, France), or rabbit anti-MFGE8 peptide (GKAEYVRAYKVAYS) (1: 1000; ProteoGenix, Schiltigheim, France), and sequentially washed 5 min in TBS, 0.1% Tween-20. The membranes were then incubated 1 h in the blocking solution, 0.1% Tween-20 and AlexaFluor® 680 goat anti-rabbit



secondary antibody (1: 20,000, Invitrogen, Carlsbad, USA), washed three times in TBS, 0.1% Tween-20 and two times in TBS. Immunobands were revealed with Odyssey® imaging system (LI-COR, Bad Homburg, Germany) with the 700 nm channel.

### Gene expression analysis

Total RNA was extracted from frozen samples (B, D, K, L, Ma, WI, RI, Ut). RNAs from K, D, Ma, WI, RI and Ut were extracted using NucleoSpin RNA® commercial kit (Macherey-Nagel, Düren, Germany), whereas B total RNA was extracted using RNA now® (Ozyme, Montigny-le Bretonneux, France) and tandem TRIreagent®-TRIreagent LS® commercial kits (Sigma-Aldrich, Saint-Quentin Fallavier, France). Tissues were extracted at 10 h p.o., except for tibial bone, as this sample was solely collected at 18 h p.o.. Additionally, Ut and RI samples were extracted at all stages (5, 6, 7, 10 and 16 h p.o.). Total RNAs from each sample were treated with TURBO DNA-free kit (Invitrogen, Carlsbad, USA). RNA concentration was measured at 260 nm and their integrity was assessed on 1.5 % agarose gels. Total RNA samples (1 µg) were reverse-transcribed using RNase H-MMLV reverse transcriptase (Superscript II, Invitrogen, Carlsbad, USA) and Oligo (dT)<sup>TM</sup> primers (Invitrogen, Carlsbad, USA).

Primers to detect expression of *Gallus gallus edil3*, *mfge8* and eight housekeeping genes (*b2m*, *ef3i*, *gapdh*, *gusb*, *stag2*, *tbp*, *sdha*, and *ppia*) were designed using Primer-BLAST (NCBI, <https://www.ncbi.nlm.nih.gov/>) (Table S4) and synthesised (Eurogentec, Liège, Belgium). Their efficiencies were evaluated by real-time quantitative RT-PCR using LightCycler® 480 SYBR Green I Master and LightCycler® 480 instrument II (Roche, Bâle, Switzerland). *Edil3*, *mfge8* and housekeeping gene expressions were quantified using the Biomark microfluidic system from Fluidigm, in which every sample-gene combination was quantified using a 96.96 Dynamic Array<sup>TM</sup> IFCs (BMK-M-96.96, Fluidigm, San Francisco, USA) at the Get-Genotoul platform (Toulouse, France). After specific pre-amplification and according to manufacturer specifications, the PCR was performed using the following thermal protocol: Thermal Mix of 50 °C, 2 min; 70 °C, 30 min; 25°C, 10 min, Hot Start at 50 °C, 2 min; 95°C, 10 min, PCR Cycle of 35 cycles of (95 °C, 15 s; 60 °C, 60 s), and melting analysis

(60°C, 30s; 95°C, 1°C/3s). RT-qPCR results were analysed using Fluidigm real-time PCR analysis software v.4.1.3 (<https://www.fluidigm.com/software>). Six biological replicates and two technical replicates were performed for each sample. GenNorm software was used for validation of housekeeping gene stabilities. *Edil3* and *mfge8* normalised quantities were calculated using the following formula: gene efficiency <sup>(ctcalibreur-ctsample)</sup> / geometric average quantity of housekeeping genes. Normalised quantities of *edil3* and *mfge8* gene transcripts were compared between various measured tissues and oviduct parts using one-way ANOVA and Tukey pairwise test analysis on Minitab® 18 software (<http://www.minitab.com/fr-fr/>) with p-value < 0.05 to detect significance.

### Synten and phylogeny of EDIL3 and MFGE8

Synten of *edil3* and *mfge8* genes were analysed using the Genome data viewer of NCBI for 8 vertebrate species (3 mammals, 2 birds, 1 non-avian reptile, 1 amphibian and 2 fishes).

EDIL3 and MFGE8 protein sequences of 12 vertebrate and 7 non-vertebrate species (Table S3) were aligned using clustalΩ multiple alignment in MEGA7(108). The appropriate substitution model, determined using MEGA7 substitution model, was LG model. The phylogenetic tree was built with MEGA7 using Maximum Likelihood method (LG substitution model) with 1,000 repetitions and the bootstrap method to evaluate branch robustness. Additionally, phylogenetic analysis using Bayesian inference was performed using BEAST v1.10.4 (109) with 10,000,000 generations and a sampling of tree each 1,000 steps. Trees were then summarised with TreeAnnotator (distributed with BEAST v1.10.4) and displayed using FigTree v1.4.4 (<http://tree.bio.ed.ac.uk/software/figtree/>).

Divergence times between species were determined using Timetree ([www.timetree.org/](http://www.timetree.org/)) and are reported on the generated phylogenetic tree.

Distinct protein domain conservation throughout the evolution of eumetazoans was investigated with HomoloGene (NCBI) and domain sequence analysis in several databases and genome browsers (ExPASy-PROSITE, <https://prosite.expasy.org/>; Ensembl, <https://www.ensembl.org/index.html>; SMART, <http://smart.embl-heidelberg.de/>).



### Analysis of gene and protein sequences of EDIL3 and MFGE8 in Gallus gallus

*Gallus gallus* *edil3* and *mfge8* gene, mRNA and protein sequences were collected from the NCBI database (*edil3* Gene ID: 427326; *edil3* transcripts: XM\_424906.6 and XM\_004949448.3; EDIL3 proteins: XP\_424906.3 and XP\_004949505.1; and *mfge8* Gene ID: 415494; *mfge8* transcripts: NM\_001277110.1 and NM\_001277111.1; MFGE8 proteins: NP\_001264039.1 and NP\_001264040.1). NCBI Genome data viewer was used in order to identify the exon / intron boundaries, and alternative splicing of each gene. EDIL3 / MFGE8 (XP\_424906.3 / NP\_001264039.1), HAPLN1 / HAPLN3 (XP\_015136083.1 / XP\_413868.3) and VCAN / ACAN (XP\_015136071.1 / XP\_015147464.1) pairwise alignments were performed using ClustalΩ in MEGA7. BioEdit software (<http://www.mbio.ncsu.edu/BioEdit/bioedit.html>) was used to determine identity and similarity percentages between sequences. Protein domains were characterised using PROSITE (<https://prosite.expasy.org/>) and NCBI graphical view. *Gallus gallus* EDIL3 and MFGE8 residues involved in Ca<sup>2+</sup>-binding site and PS-binding were identified by homology with *Homo sapiens* coagulation factor IX and X EGF domain residues and *Mus musculus* MFGE8 second F5/8C domain residues (28,110). Alignment of *Gallus gallus* EDIL3 (XP\_424906.3) and MFGE8 (NP\_001264039.1) F5/8C 2 with *Mus musculus* MFGE8 (NP\_001038954.1) F5/8C 2 was performed using ClustalΩ (<https://www.ebi.ac.uk/Tools/msa/clustalo/>)

### *Gallus gallus* EDIL3 and MFGE8 secondary and tertiary structure homology

Secondary structure of *Gallus gallus* EDIL3 (XP\_424906.3) and MFGE8 (NP\_001264039.1) peptide signal regions was predicted using PSIPRED v3.3 (<http://bioinf.cs.ucl.ac.uk/psipred/>). EGF-like and F5/8C sequence regions were then loaded on the I-TASSER program server (111) (<https://zhanglab.ccmb.med.umich.edu/I-TASSER/>), to generate secondary and tertiary structural predictions. This template-based modelling program computed protein 3D structure predictions by molecular homology for each region of EDIL3 and MFGE8. The 3D structure prediction models were edited on

PyMOL Molecular Graphics system (<https://pymol.org/2/>).

### Purification of extracellular vesicles from uterine fluid, examination by transmission electron microscopy and energy dispersive X-ray analysis

Immediately after dilution, EVs were isolated from UF harvested at 7 h p.o., using previously described methodology (112). Briefly, diluted UFs were centrifuged at 100 x g for 15 min and then at 12,000 g for 15 min to remove cell debris (Sorvall ST40 R, Thermo Fisher Scientific, Waltham, USA). Two successive ultracentrifugation steps at 100,000 g (Beckman Coulter L8-70M, Beckman, Fullerton, USA) were then performed during 90 min to pellet the EVs. The pellet was suspended in 50 µL of PBS and stored at -20°C until transmission electron microscopy (TEM) analysis.

Ten microliters of EV fraction were deposited on an electron microscope grid (Copper + Carbon) and then dried for 1 min. Excess liquid was absorbed with filter paper and EVs were stained with uranyl acetate 2 %. The grid was then immediately observed with TEM-1400 Plus electron microscope (120 kV; JEOL, Tokyo, Japan). Additionally, frozen beads (20 µL) of uterine fluid harvested at 16 h p.o. and negatively stained with uranyl acetate 2 % were deposited on electron microscope grids and Energy dispersive X-ray (EDS, Oxford 65 mm<sup>2</sup> detector, Aztec software) measurements were performed in order to detect calcium, oxygen and carbon.

**Acknowledgements:** The authors are grateful to Jacky Ezagal for his technical skills and his help in molecular biology experiments. The authors also thank the experimental unit (UE-PEAT) for the care of birds, the GeT-GenoToul platform Toulouse for performing the real time quantitative PCR with the Biomark Fluidigm system and Pierre-Ivan Raynal and Sonia Georgeault from electronic microscopy Platform of the Université François Rabelais de Tours for the microscopic observations. MH's participation was partially supported by the Canadian Natural Sciences and Engineering Research Council (NSERC, Discovery program RGPIN-2016-04410).

The authors wish to thank the Université François Rabelais de Tours and the Région Centre Val de Loire for financial support of Lilian Stapane's doctoral studies.

**Conflict of interest:** The authors declare that they have no conflicts of interest with the contents of this article.

**Author contributions:** LS was involved in designing and planning of the study. He carried out the bibliographic investigations, experiments and analysis, interpreted data, annotation and all analysis and wrote the paper. NLR was fully involved in the management support of LS (PhD student). She was involved in the experimental design, analysis and management of the study, and contributed to the writing of the paper. MH was involved in the strategy and contributed to the writing of the paper and made critical reading and editing of the manuscript. JG is the supervisor of LS (PhD student). He conceived the strategy, performed the design, interpreted data, annotation and statistical analyses and was fully involved in the writing of the paper. All authors have read and approved the final manuscript.

## References

1. Nys, Y., Gautron, J., Garcia-Ruiz, J. M., and Hincke, M. T. (2004) Avian eggshell mineralization: biochemical and functional characterization of matrix proteins. *Cr Palevol* **3**, 549-562
2. Hincke, M. T., Nys, Y., Gautron, J., Mann, K., Rodriguez-Navarro, A. B., and McKee, M. D. (2012) The eggshell: structure, composition and mineralization. *Front Biosci (Landmark Ed)* **17**, 1266-1280
3. Hamilton, R. M. G. (1986) The Microstructure of the Hens Eggshell - a Short Review. *Food Microstruct* **5**, 99-110
4. Arias, J. L., Fink, D. J., Xiao, S. Q., Heuer, A. H., and Caplan, A. I. (1993) Biomineralization and eggshells: cell-mediated acellular compartments of mineralized extracellular matrix. *Int Rev Cytol* **145**, 217-250
5. Nys, Y., Hincke, M. T., Arias, J. L., Garcia-Ruiz, J. M., and Solomon, S. E. (1999) Avian eggshell mineralization. *Poult Avian Biol Rev* **10**, 143-166
6. Rodriguez-Navarro, A. B., Marie, P., Nys, Y., Hincke, M. T., and Gautron, J. (2015) Amorphous calcium carbonate controls avian eggshell mineralization: A new paradigm for understanding rapid eggshell calcification. *J Struct Biol* **190**, 291-303
7. Gautron, J., Hincke, M. T., and Nys, Y. (1997) Precursor matrix proteins in the uterine fluid change with stages of eggshell formation in hens. *Connect Tissue Res* **36**, 195-210
8. Jonchere, V., Brionne, A., Gautron, J., and Nys, Y. (2012) Identification of uterine ion transporters for mineralisation precursors of the avian eggshell. *BMC Physiol* **12**, 10
9. Dominguez-Vera, J. M., Gautron, J., Garcia-Ruiz, J. M., and Nys, Y. (2000) The effect of avian uterine fluid on the growth behavior of calcite crystals. *Poult Sci* **79**, 901-907
10. Hernandez-Hernandez, A., Gomez-Morales, J., Rodriguez-Navarro, A. B., Gautron, J., Nys, Y., and Garcia-Ruiz, J. M. (2008) Identification of Some Active Proteins in the Process of Hen Eggshell Formation. *Cryst Growth Des* **8**, 4330-4339
11. Mann, K., Macek, B., and Olsen, J. V. (2006) Proteomic analysis of the acid-soluble organic matrix of the chicken calcified eggshell layer. *Proteomics* **6**, 3801-3810
12. Mann, K., Olsen, J. V., Macek, B., Gnad, F., and Mann, M. (2007) Phosphoproteins of the chicken eggshell calcified layer. *Proteomics* **7**, 106-115
13. Miksik, I., Sedlakova, P., Lacinova, K., Pataridis, S., and Eckhardt, A. (2010) Determination of insoluble avian eggshell matrix proteins. *Analytical and Bioanalytical Chemistry* **397**, 205-214
14. Rose-Martel, M., Du, J. W., and Hincke, M. T. (2012) Proteomic analysis provides new insight into the chicken eggshell cuticle. *J Proteomics* **75**, 2697-2706
15. Sun, C., Xu, G., and Yang, N. (2013) Differential label-free quantitative proteomic analysis of avian eggshell matrix and uterine fluid proteins associated with eggshell mechanical property. *Proteomics* **13**, 3523-3536
16. Kaweewong, K., Garnjanagoonchorn, W., Jirapakkul, W., and Roytrakul, S. (2013) Solubilization and identification of hen eggshell membrane proteins during different times of chicken embryo development using the proteomic approach. *Protein J* **32**, 297-308
17. Miksik, I., Ergang, P., and Pacha, J. (2014) Proteomic analysis of chicken eggshell cuticle membrane layer. *Anal Bioanal Chem* **406**, 7633-7640
18. Ahmed, T. A., Suso, H. P., and Hincke, M. T. (2017) In-depth comparative analysis of the chicken eggshell membrane proteome. *J Proteomics* **155**, 49-62
19. Marie, P., Labas, V., Brionne, A., Harichaux, G., Hennequet-Antier, C., Nys, Y., and Gautron, J. (2015) Quantitative proteomics and bioinformatic analysis provide new insight into protein function during avian eggshell biomineralization. *J Proteomics* **113**, 178-193
20. Gautron, J., Guyot, N., Brionne, A., and Réhault-Godbert, S. (2019) Bioactive Minor Egg Components. in *Eggs as Functional Foods and Nutraceuticals for Human Health* (Chemistry, T. R. S. o. ed.). pp 259-284
21. Marie, P., Labas, V., Brionne, A., Harichaux, G., Hennequet-Antier, C., Rodriguez-Navarro, A. B., Nys, Y., and Gautron, J. (2015) Quantitative proteomics provides new insights into chicken

- eggshell matrix protein functions during the primary events of mineralisation and the active calcification phase. *J Proteomics* **126**, 140-154
22. Brionne, A., Nys, Y., Hennequet-Antier, C., and Gautron, J. (2014) Hen uterine gene expression profiling during eggshell formation reveals putative proteins involved in the supply of minerals or in the shell mineralization process. *Bmc Genomics* **15**
  23. Mann, K., and Mann, M. (2013) The proteome of the calcified layer organic matrix of turkey (*Meleagris gallopavo*) eggshell. *Proteome Sci* **11**
  24. Mann, K., and Mann, M. (2015) Proteomic analysis of quail calcified eggshell matrix: a comparison to chicken and turkey eggshell proteomes. *Proteome Sci* **13**, 22
  25. Le Roy, N., Combes-Soia, L., Brionne, A., Labas, V., Rodriguez-Navarro, A., Hincke, M., Nys, Y., and Gautron, J. (2019) Guinea fowl eggshell quantitative proteomics yield new findings related to its unique structural characteristics and superior mechanical properties. *J Proteomics*, Submitted
  26. Oshima, K., Aoki, N., Negi, M., Kishi, M., Kitajima, K., and Matsuda, T. (1999) Lactation-dependent expression of an mRNA splice variant with an exon for a multiply O-glycosylated domain of mouse milk fat globule glycoprotein MFG-E8. *Biochem Bioph Res Co* **254**, 522-528
  27. Oshima, K., Yasueda, T., Nishio, S., and Matsuda, T. (2014) MFG-E8: Origin, Structure, Expression, Functions and Regulation. in *MFG-E8 and Inflammation* (Nature, S. ed.). pp 1-31
  28. Ye, H., Li, B. H., Subramanian, V., Choi, B. H., Liang, Y., Harikishore, A., Chakraborty, G., Baek, K., and Yoon, H. S. (2013) NMR solution structure of C2 domain of MFG-E8 and insights into its molecular recognition with phosphatidylserine. *Bba-Biomembranes* **1828**, 1083-1093
  29. Stubbs, J. D., Lekutis, C., Singer, K. L., Bui, A., Yuzuki, D., Srinivasan, U., and Parry, G. (1990) Cdna Cloning of a Mouse Mammary Epithelial-Cell Surface Protein Reveals the Existence of Epidermal Growth Factor-Like Domains Linked to Factor-Viii-Like Sequences. *P Natl Acad Sci USA* **87**, 8417-8421
  30. Thery, C., Regnault, A., Garin, J., Wolfers, J., Zitvogel, L., Ricciardi-Castagnoli, P., Raposo, G., and Amigorena, S. (1999) Molecular characterization of dendritic cell-derived exosomes: Selective accumulation of the heat shock protein hsc73. *J Cell Biol* **147**, 599-610
  31. Hanayama, R., Tanaka, M., Miwa, K., Shinohara, A., Iwamatsu, A., and Nagata, S. (2002) Identification of a factor that links apoptotic cells to phagocytes. *Nature* **417**, 182-187
  32. Ensslin, M. A., and Shur, B. D. (2003) Identification of mouse sperm SED1, a bimotif EGF repeat and discoidin-domain protein involved in sperm-egg binding. *Cell* **114**, 405-417
  33. Gatti, J. L., Metayer, S., Belghazi, M., Dacheux, F., and Dacheux, J. L. (2005) Identification, proteomic profiling, and origin of ram epididymal fluid exosome-like vesicles. *Biol Reprod* **72**, 1452-1465
  34. Ait-Oufella, H., Kinugawa, K., Zoll, J., Simon, T., Boddaert, J., Heeneman, S., Blanc-Brude, O., Barateau, V., Potteaux, S., Merval, R., Esposito, B., Teissier, E., Daemen, M. J., Leseche, G., Boulanger, C., Tedgui, A., and Mallat, Z. (2007) Lactadherin deficiency leads to apoptotic cell accumulation and accelerated atherosclerosis in mice. *Circulation* **115**, 2168-2177
  35. Hidai, C., Zupancic, T., Penta, K., Mikhail, A., Kawana, M., Quertermous, E. E., Aoka, Y., Fukagawa, M., Matsui, Y., Platika, D., Auerbach, R., Hogan, B. L. M., Snodgrass, R., and Quertermous, T. (1998) Cloning and characterization of developmental endothelial locus-1: An embryonic endothelial cell protein that binds the alpha v beta 3 integrin receptor. *Gene Dev* **12**, 21-33
  36. Penta, K., Varner, J. A., Liaw, L., Hidai, C., Schatzman, R., and Quertermous, T. (1999) Del1 induces integrin signaling and angiogenesis by ligation of alpha V beta 3. *J Biol Chem* **274**, 11101-11109
  37. Zhong, J. P., Eliceiri, B., Stupack, D., Penta, K., Sakamoto, G., Quertermous, T., Coleman, M., Boudreau, N., and Varner, J. A. (2003) Neovascularization of ischemic tissues by gene delivery of the extracellular matrix protein Del-1. *J Clin Invest* **112**, 30-41



38. Zou, X. L., Qiao, H. Q., Jiang, X. A., Dong, X. S., Jiang, H. C., and Sun, X. Y. (2008) Downregulation of developmentally regulated endothelial cell locus-1 inhibits the growth of colon cancer. *J Biomed Sci* **16**
39. Aoka, Y., Johnson, F. L., Penta, K., Hirata, K., Hidai, C., Schatzman, R., Varner, J. A., and Quertermous, T. (2002) The embryonic angiogenic factor Del1 accelerates tumor growth by enhancing vascular formation. *Microvasc Res* **64**, 148-161
40. Lee, J. E., Moon, P. G., Cho, Y. E., Kim, Y. B., Kim, I. S., Park, H. Y., and Baek, M. C. (2016) Identification of EDIL3 on extracellular vesicles involved in breast cancer cell invasion. *J Proteomics* **131**, 17-28
41. Pavlopoulou, A., Pampalakis, G., Michalopoulos, I., and Sotiropoulou, G. (2010) Evolutionary history of tissue kallikreins. *PLoS One* **5**, e13781
42. Packard, M. J., and Seymour, R. S. (1997) Evolution of the amniote egg. in *Amniote Origins* (Press, A. ed.), Sumida, S.S., and K.L.M. Martin pp 265–290
43. Romer, A. S. (1957) Origin of the amniote egg. *The Scientific Monthly* **85**, 57-63
44. Larocca, D., Peterson, J. A., Urrea, R., Kuniyoshi, J., Bistrain, A. M., and Ceriani, R. L. (1991) A Mr 46,000 Human-Milk Fat Globule Protein That Is Highly Expressed in Human Breast-Tumors Contains Factor-Viii-Like Domains. *Cancer Res* **51**, 4994-4998
45. Andersen, M. H., Berglund, L., Rasmussen, J. T., and Petersen, T. E. (1997) Bovine PAS-6/7 binds alpha(V)beta(5) integrin and anionic phospholipids through two domains. *Biochemistry-Us* **36**, 5441-5446
46. Shi, J., Heegaard, C. W., Rasmussen, J. T., and Gilbert, G. E. (2004) Lactadherin binds selectively to membranes containing phosphatidyl-L-serine and increased curvature. *Biochim Biophys Acta* **1667**, 82-90
47. Otzen, D. E., Blans, K., Wang, H. B., Gilbert, G. E., and Rasmussen, J. T. (2012) Lactadherin binds to phosphatidylserine-containing vesicles in a two-step mechanism sensitive to vesicle size and composition. *Bba-Biomembranes* **1818**, 1019-1027
48. Shao, C., Novakovic, V. A., Head, J. F., Seaton, B. A., and Gilbert, G. E. (2008) Crystal structure of lactadherin C2 domain at 1.7A resolution with mutational and computational analyses of its membrane-binding motif. *J Biol Chem* **283**, 7230-7241
49. Oshima, K., Aoki, N., Kato, T., Kitajima, K., and Matsuda, T. (2002) Secretion of a peripheral membrane protein, MFG-E8, as a complex with membrane vesicles. *Eur J Biochem* **269**, 1209-1218
50. Podlaha, O., Webb, D. M., and Zhang, J. (2006) Accelerated evolution and loss of a domain of the sperm-egg-binding protein SED1 in ancestral primates. *Mol Biol Evol* **23**, 1828-1831
51. Hvarregaard, J., Andersen, M. H., Berglund, L., Rasmussen, J. T., and Petersen, T. E. (1996) Characterization of glycoprotein PAS-6/7 from membranes of bovine milk fat globules. *European Journal of Biochemistry* **240**, 628-636
52. Gautron, J. (2018) ANR IMPACT report.
53. Gautron, J., Brionne, A., Bouchez, O., Cabau, C., Antier-Hennequet, C., Hincke, M., and Nys, Y. An integrative study of gene and protein toolkits of chicken eggshell biomineralization. in preparation
54. Raymond, A., Ensslin, M. A., and Shur, B. D. (2009) SED1/MFG-E8: A Bi-Motif Protein That Orchestrates Diverse Cellular Interactions. *J Cell Biochem* **106**, 957-966
55. Nys, Y., and Guyot, N. (2011) Egg formation and chemistry. in *Improving the safety and quality of eggs and egg products* (publishing, W. ed.). pp 83-132
56. Nys, Y., Parkes, C. O., and Thomasset, M. (1986) Effects of suppression and resumption of shell formation and parathyroid hormone on uterine calcium-binding protein, carbonic anhydrase activity, and intestinal calcium absorption in hens. *Gen Comp Endocrinol* **64**, 293-299
57. Ankra-Badu, G., and Aggrey, S. (2005) Identification of candidate genes at quantitative trait loci on chicken Chromosome Z using orthologous comparison of chicken, mouse, and human genomes. *Poultry Sci* **84**, 50-50

58. Tuiskula-Haavisto, M., Honkatukia, M., Vilkkii, J., de Koning, D. J., Schulman, N. F., and Maki-Tanila, A. (2002) Mapping of quantitative trait loci affecting quality and production traits in egg layers. *Poultry Sci* **81**, 919-927
59. Cordeiro, C. M. M., and Hincke, M. T. (2016) Quantitative proteomics analysis of eggshell membrane proteins during chick embryonic development. *J Proteomics* **130**, 11-25
60. Carrino, D. A., Dennis, J. E., Wu, T. M., Arias, J. L., Fernandez, M. S., Rodriguez, J. P., Fink, D. J., Heuer, A. H., and Caplan, A. I. (1996) The avian eggshell extracellular matrix as a model for biomineralization. *Connective Tissue Research* **35**, 325-328
61. Fernandez, M. S., Araya, M., and Arias, J. L. (1997) Eggshells are shaped by a precise spatio-temporal arrangement of sequentially deposited macromolecules. *Matrix Biol* **16**, 13-20
62. Nakano, T., Ikawa, N., and Ozimek, L. (2001) Extraction of glycosaminoglycans from chicken eggshell. *Poult Sci* **80**, 681-684
63. Nakano, T., Ikawa, N., and Ozimek, L. (2002) Galactosaminoglycan composition in chicken eggshell. *Poult Sci* **81**, 709-714
64. Hunter, G. K., Wong, K. S., and Kim, J. J. (1988) Binding of calcium to glycosaminoglycans: an equilibrium dialysis study. *Arch Biochem Biophys* **260**, 161-167
65. Kiani, C., Chen, L., Wu, Y. J., Yee, A. J., and Yang, B. B. (2002) Structure and function of aggrecan. *Cell Res* **12**, 19-32
66. Shibata, S., Fukada, K., Imai, H., Abe, T., and Yamashita, Y. (2003) In situ hybridization and immunohistochemistry of versican, aggrecan and link protein, and histochemistry of hyaluronan in the developing mouse limb bud cartilage. *J Anat* **203**, 425-432
67. Matsumoto, K., Kamiya, N., Suwan, K., Atsumi, F., Shimizu, K., Shinomura, T., Yamada, Y., Kimata, K., and Watanabe, H. (2006) Identification and characterization of versican/PD-M aggregates in cartilage. *J Biol Chem* **281**, 18257-18263
68. Anderson, H. C. (1969) Vesicles associated with calcification in the matrix of epiphyseal cartilage. *J Cell Biol* **41**, 59-72
69. Xiao, Z., Camalier, C. E., Nagashima, K., Chan, K. C., Lucas, D. A., de la Cruz, M. J., Gignac, M., Lockett, S., Issaq, H. J., Veenstra, T. D., Conrads, T. P., and Beck, G. R., Jr. (2007) Analysis of the extracellular matrix vesicle proteome in mineralizing osteoblasts. *J Cell Physiol* **210**, 325-335
70. Golub, E. E. (2009) Role of matrix vesicles in biomineralization. *Biochim Biophys Acta* **1790**, 1592-1598
71. Morhayim, J., Baroncelli, M., and van Leeuwen, J. P. (2014) Extracellular vesicles: specialized bone messengers. *Arch Biochem Biophys* **561**, 38-45
72. Bottini, M., Mebarek, S., Anderson, K. L., Strzelecka-Kiliszek, A., Bozycki, L., Simao, A. M. S., Bolean, M., Ciancaglini, P., Pikula, J. B., Pikula, S., Magne, D., Volkmann, N., Hanein, D., Millan, J. L., and Buchet, R. (2018) Matrix vesicles from chondrocytes and osteoblasts: Their biogenesis, properties, functions and biomimetic models. *Biochim Biophys Acta Gen Subj* **1862**, 532-546
73. Hasegawa, T., Yamamoto, T., Tsuchiya, E., Hongo, H., Tsuboi, K., Kudo, A., Abe, M., Yoshida, T., Nagai, T., Khadiza, N., Yokoyama, A., Oda, K., Ozawa, H., de Freitas, P. H. L., Li, M., and Amizuka, N. (2017) Ultrastructural and biochemical aspects of matrix vesicle-mediated mineralization. *Jpn Dent Sci Rev* **53**, 34-45
74. Mahamid, J., Sharir, A., Gur, D., Zelzer, E., Addadi, L., and Weiner, S. (2011) Bone mineralization proceeds through intracellular calcium phosphate loaded vesicles: A cryo-electron microscopy study. *J Struct Biol* **174**, 527-535
75. Kerschnitzki, M., Akiva, A., Ben Shoham, A., Asscher, Y., Wagermaier, W., Fratzl, P., Addadi, L., and Weiner, S. (2016) Bone mineralization pathways during the rapid growth of embryonic chicken long bones. *J Struct Biol* **195**, 82-92
76. Kerschnitzki, M., Akiva, A., Ben Shoham, A., Koifman, N., Shimon, E., Rechav, K., Arraf, A. A., Schultheiss, T. M., Talmon, Y., Zelzer, E., Weiner, S., and Addadi, L. (2016) Transport of membrane-bound mineral particles in blood vessels during chicken embryonic bone development. *Bone* **83**, 65-72

77. Balcerzak, M., Malinowska, A., Thouverey, C., Sekrecka, A., Dadlez, M., Buchet, R., and Pikula, S. (2008) Proteome analysis of matrix vesicles isolated from femurs of chicken embryo. *Proteomics* **8**, 192-205
78. Rosenthal, A. K., Gohr, C. M., Ninomiya, J., and Wakim, B. T. (2011) Proteomic Analysis of Articular Cartilage Vesicles From Normal and Osteoarthritic Cartilage. *Arthritis Rheum-Us* **63**, 401-411
79. Shapiro, I. M., Landis, W. J., and Risbud, M. V. (2015) Matrix vesicles: Are they anchored exosomes? *Bone* **79**, 29-36
80. Thouverey, C., Malinowska, A., Balcerzak, M., Strzelecka-Kiliszek, A., Buchet, R., Dadlez, M., and Pikula, S. (2011) Proteomic characterization of biogenesis and functions of matrix vesicles released from mineralizing human osteoblast-like cells. *J Proteomics* **74**, 1123-1134
81. Waqas, M. Y., Yang, P., Ahmed, N., Zhang, Q., Liu, T., Li, Q., Hu, L., Hong, C., and Chen, Q. (2016) Characterization of the ultrastructure in the uterovaginal junction of the hen. *Poultry Sci* **95**, 2112-2119
82. Hincke, M. T., Chien, Y. C., Gerstenfeld, L. C., and McKee, M. D. (2008) Colloidal-gold immunocytochemical localization of osteopontin in avian eggshell gland and eggshell. *J Histochem Cytochem* **56**, 467-476
83. Chien, Y. C., Hincke, M. T., and McKee, M. D. (2009) Ultrastructure of avian eggshell during resorption following egg fertilization. *J Struct Biol* **168**, 527-538
84. Wyburn, G. M., Johnston, H. S., Draper, M. H., and Davidson, M. F. (1973) The ultrastructure of the shell forming region of the oviduct and the development of the shell of *Gallus domesticus*. *Q J Exp Physiol Cogn Med Sci* **58**, 143-151
85. Dennis, J. E., Xiao, S. Q., Agarwal, M., Fink, D. J., Heuer, A. H., and Caplan, A. I. (1996) Microstructure of matrix and mineral components of eggshells from White Leghorn chickens (*Gallus gallus*). *J Morphol* **228**, 287-306
86. Fraser, A. C., Bain, M. M., and Solomon, S. E. (1998) Organic matrix morphology and distribution in the palisade layer of eggshells sampled at selected periods during lay. *Brit Poultry Sci* **39**, 225-228
87. Hincke, M. T., Gautron, J., Tsang, C. P. W., McKee, M. D., and Nys, Y. (1999) Molecular cloning and ultrastructural localization of the core protein of an eggshell matrix proteoglycan, ovocleidin-116. *J Biol Chem* **274**, 32915-32923
88. Brecevic, L., and Nielsen, A. E. (1989) Solubility of Amorphous Calcium-Carbonate. *J Cryst Growth* **98**, 504-510
89. Addadi, L., Raz, S., and Weiner, S. (2003) Taking advantage of disorder: Amorphous calcium carbonate and its roles in biomineralization. *Adv Mater* **15**, 959-970
90. Weiss, I. M., Tuross, N., Addadi, L., and Weiner, S. (2002) Mollusc larval shell formation: Amorphous calcium carbonate is a precursor phase for aragonite. *J Exp Zool* **293**, 478-491
91. Luquet, G. (2012) Biomineralizations: insights and prospects from crustaceans. *Zookeys*, 103-121
92. Tester, C. C., Brock, R. E., Wu, C. H., Krejci, M. R., Weigand, S., and Joester, D. (2011) In vitro synthesis and stabilization of amorphous calcium carbonate (ACC) nanoparticles within liposomes. *Crystengcomm* **13**, 3975-3978
93. Nys, Y., Zawadzki, J., Gautron, J., and Mills, A. D. (1991) Whitening of brown-shelled eggs: mineral composition of uterine fluid and rate of protoporphyrin deposition. *Poult Sci* **70**, 1236-1245
94. Vidavsky, N., Masic, A., Schertel, A., Weiner, S., and Addadi, L. (2015) Mineral-bearing vesicle transport in sea urchin embryos. *J Struct Biol* **192**, 358-365
95. Kirsch, T., Harrison, G., Golub, E. E., and Nah, H. D. (2000) The roles of annexins and types II and X collagen in matrix vesicle-mediated mineralization of growth plate cartilage. *J Biol Chem* **275**, 35577-35583

96. Genge, B. R., Wu, L. N., and Wuthier, R. E. (2007) In vitro modeling of matrix vesicle nucleation: synergistic stimulation of mineral formation by annexin A5 and phosphatidylserine. *J Biol Chem* **282**, 26035-26045
97. Merolli, A., and Santin, M. (2009) Role of phosphatidyl-serine in bone repair and its technological exploitation. *Molecules* **14**, 5367-5381
98. Rojas, E., Arispe, N., Haigler, H. T., Burns, A. L., and Pollard, H. B. (1992) Identification of Annexins as Calcium Channels in Biological-Membranes. *Bone Miner* **17**, 214-218
99. Wuthier, R. E., Wu, L. N. Y., Sauer, G. R., Genge, B. R., Yoshimori, T., and Ishikawa, Y. (1992) Mechanism of Matrix Vesicle Calcification - Characterization of Ion Channels and the Nucleational Core of Growth Plate Vesicles. *Bone Miner* **17**, 290-295
100. Kirsch, T., Nah, H. D., Demuth, D. R., Harrison, G., Golub, E. E., Adams, S. L., and Pacifici, M. (1997) Annexin V-mediated calcium flux across membranes is dependent on the lipid composition: Implications for cartilage mineralization. *Biochemistry-Us* **36**, 3359-3367
101. Zhu, F., Zhang, F., Hincke, M., Yin, Z. T., Chen, S. R., Yang, N., and Hou, Z. C. (2019) iTRAQ-Based Quantitative Proteomic Analysis of Duck Eggshell During Biomineralization. *Proteomics*, e1900011
102. Arad, Z., Eylath, U., Ginsburg, M., and Eyal-Giladi, H. (1989) Changes in uterine fluid composition and acid-base status during shell formation in the chicken. *Am J Physiol* **257**, R732-737
103. Voinescu, A. E., Touraud, D., Lecker, A., Pfitzner, A., Kunz, W., and Ninham, B. W. (2007) Mineralization of CaCO<sub>3</sub> in the presence of egg white lysozyme. *Langmuir* **23**, 12269-12274
104. Pipich, V., Balz, M., Wolf, S. E., Tremel, W., and Schwahn, D. (2008) Nucleation and growth of CaCO<sub>3</sub> mediated by the egg-white protein ovalbumin: a time-resolved in situ study using small-angle neutron scattering. *J Am Chem Soc* **130**, 6879-6892
105. Freeman, C. L., Harding, J. H., Quigley, D., and Rodger, P. M. (2010) Structural Control of Crystal Nuclei by an Eggshell Protein. *Angew Chem Int Edit* **49**, 5135-5137
106. Pathan, M., Fonseka, P., Chitti, S. V., Kang, T., Sanwlan, R., Van Deun, J., Hendrix, A., and Mathivanan, S. (2019) Vesiclepedia 2019: a compendium of RNA, proteins, lipids and metabolites in extracellular vesicles. *Nucleic Acids Res* **47**, D516-D519
107. Gautron, J., Hincke, M. T., Panheleux, M., Garcia-Ruiz, J. M., Boldicke, T., and Nys, Y. (2001) Ovotransferrin is a matrix protein of the hen eggshell membranes and basal calcified layer. *Connective Tissue Research* **42**, 255-267
108. Kumar, S., Stecher, G., and Tamura, K. (2016) MEGA7: Molecular Evolutionary Genetics Analysis Version 7.0 for Bigger Datasets. *Mol Biol Evol* **33**, 1870-1874
109. Drummond, A. J., and Rambaut, A. (2007) BEAST: Bayesian evolutionary analysis by sampling trees. *Bmc Evol Biol* **7**
110. Handford, P. A., Baron, M., Mayhew, M., Willis, A., Beesley, T., Brownlee, G. G., and Campbell, I. D. (1990) The first EGF-like domain from human factor IX contains a high-affinity calcium binding site. *EMBO J* **9**, 475-480
111. Yang, J. Y., and Zhang, Y. (2015) I-TASSER server: new development for protein structure and function predictions. *Nucleic Acids Res* **43**, W174-W181
112. Thery, C., Amigorena, S., Raposo, G., and Clayton, A. (2006) Isolation and characterization of exosomes from cell culture supernatants and biological fluids. *Curr Protoc Cell Biol* **Chapter 3**, Unit 3 22



## FOOTNOTES

The abbreviations used are: ACAN, aggrecan; ACC, amorphous calcium carbonate; ANX, annexin; B, tibial bone; CA, carbonic anhydrase;  $\text{CaCO}_3$ , calcium carbonate; D, duodenum; DEL1, developmental endothelial locus-1; EDIL3, EGF-like repeats and discoidin I-like domains 3; EGF-like, epidermal growth factor-like; EV, extracellular vesicle; F5/8C, Coagulation factor 5/8 domain; HAPLN1, hyaluronan and proteoglycan link protein 1; HAPLN3, hyaluronan and proteoglycan link protein 3;  $\text{HCO}_3^-$ , bicarbonate ion; ITG, integrin; K, kidney; L, liver; Ma, magnum; MFGE8, milk fat globule-EGF factor 8; MYA, million years ago; OM, organic matrix; p.o., post-ovulation; PS, phosphatidylserine; RI, red isthmus; SEM, soluble eggshell matrix; UF, uterine fluid; Ut, uterus; VCAN, versican; WI, white isthmus.

**Table 1.** Proteins involved in the proposed vesicular transport. All proteins have been reported in proteomic studies of chicken eggshell (ES) or uterine fluid (UF) (11,15,19,21). ANX and CA can provide  $\text{Ca}^{2+}$  or  $\text{HCO}_3^-$ , respectively. ACC can be stabilised by LYZ (103), OC17 (105) or OVAL (104). Extracellular vesicle (EV) markers are from the Vesiclepedia database (106).

| Mineralising activity |   |                   | EV markers found in ES or UF |                |
|-----------------------|---|-------------------|------------------------------|----------------|
| Targeting             | Ion accumulation<br>( $\text{Ca}^{2+}$ and $\text{HCO}_3^-$ ) | ACC stabilisation | Function                     | Protein symbol |
| EDIL3                 | ANXA1   | LYZ               | Chaperone                    | HSP90AA1       |
| MFGE8                 | ANXA2   | OC17              |                              | HSP90B1        |
|                       | ANXA5   | OVAL              |                              | HSPA5          |
|                       | ANXA8   |                   |                              | HSPA8          |
|                       | CA2   |                   | Biogenesis factor            | PDCD6IP        |
|                       | CA4   |                   |                              | Syntenin-1     |
|                       |   |                   |                              | EZR            |
|                       |   |                   |                              | TSG101         |
|                       |   |                   | Cell adhesion                | FN1            |
|                       |   |                   | Intracellular trafficking    | RAB10          |
|                       |   |                   | Membrane organiser           | CD9            |
|                       |   |                   | Signalling protein           | YWHAE          |
|                       |   |                   |                              | YWHAZ          |
|                       |   |                   | Other (cargo)                | ALB            |
|                       |   |                   |                              | VCP            |
|                       |   |                   |                              | TPI1           |
|                       |   |                   |                              | GSN            |
|                       |   |                   |                              | LDHB           |
|                       |   |                   |                              | ENO1           |
|                       |   |                   |                              | GDI2           |

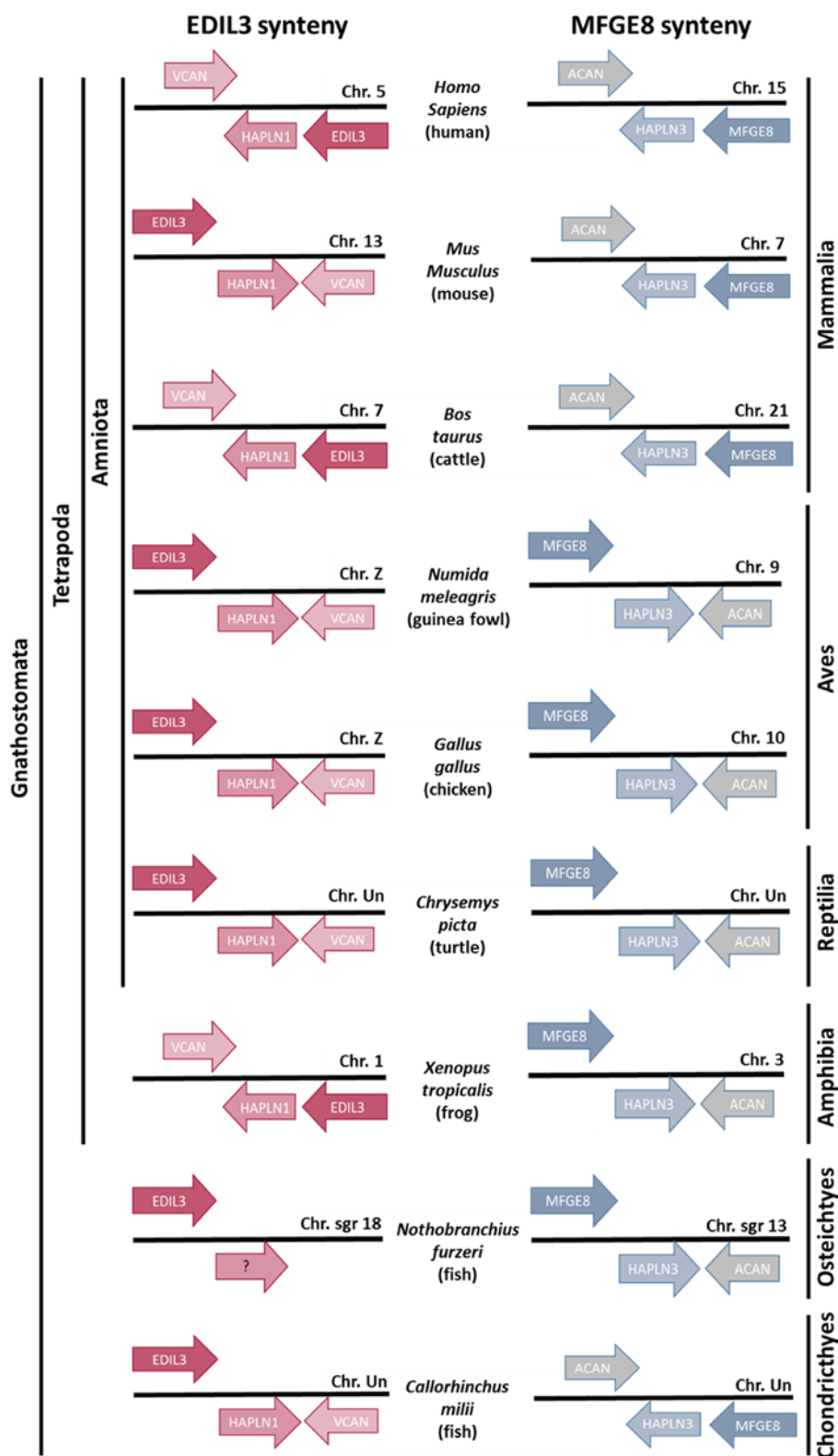


**Figure 1.** Chromosomal arrangements of *edil3* and *mfge8* gene clusters for several vertebrate classes. Gene organisation was investigated on the NCBI genome explorer. Arrows indicate the direction of gene transcription.

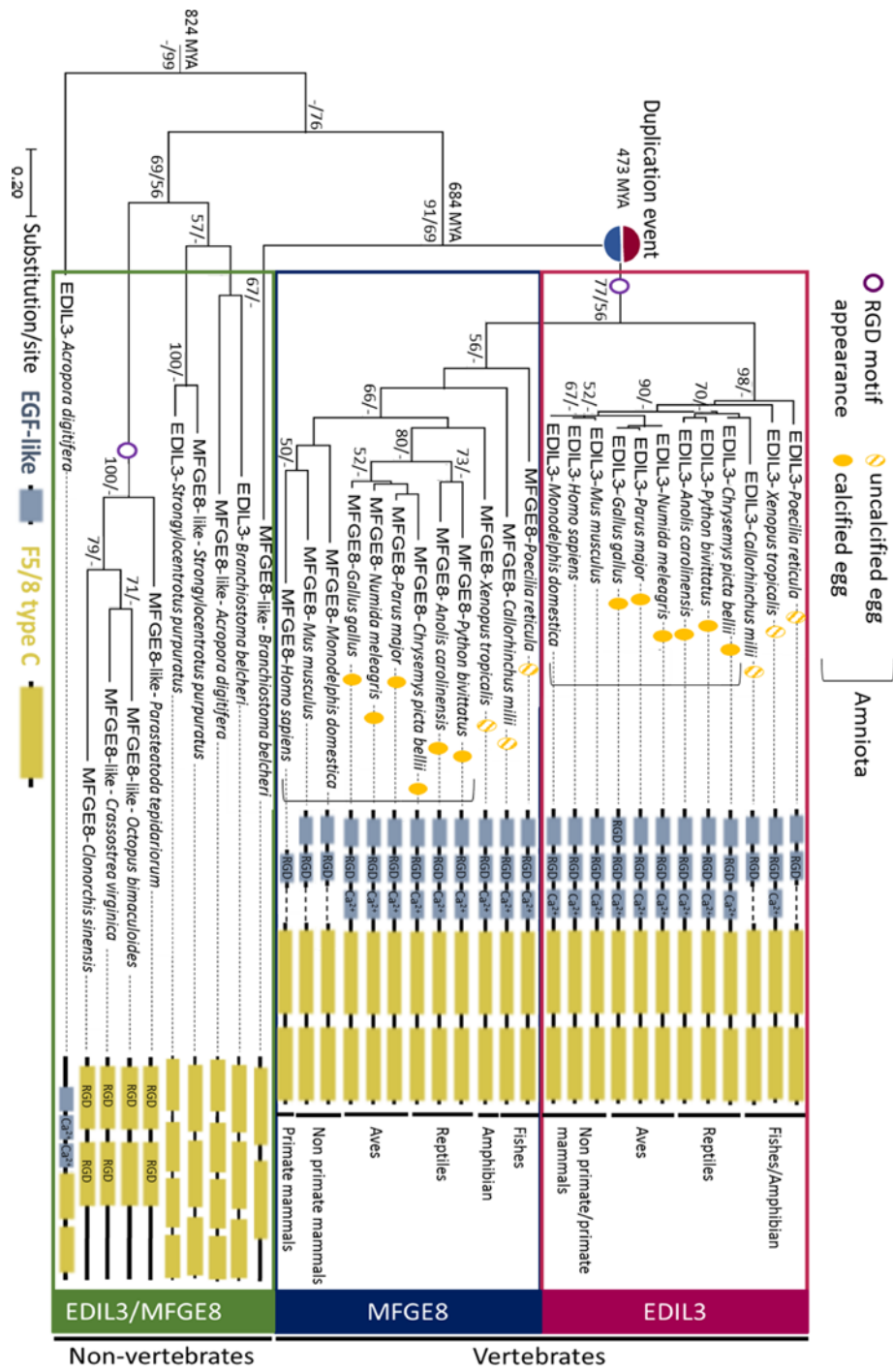


**Figure 2.** Phylogenetic tree reconstruction of EDIL3 and MFGE8 common evolutionary histories in Eumetazoa. Multiple alignment of protein sequences (LG substitution model) was performed using ClustalΩ and the phylogenetic tree was reconstructed using Maximum Likelihood (in MEGA7) and Bayesian inference (in BEAST v1.10.4) methods. The topology of the tree is that resulting from Maximum Likelihood. Node values correspond to the percentage of Maximum Likelihood bootstrap values/Bayesian posterior probabilities respectively. Only values above 50 are indicated. The divergence times were analysed on Timetree. The schematic representation of EDIL3 and MFGE8 protein domains were acquired with HomoloGene of NCBI and several databases (ExPASy-PROSITE, Ensembl and SMART). MYA: Million years ago, RGD: Integrin-binding site,  $\text{Ca}^{2+}$ : Calcium-binding site, EGF: Epidermal growth factor domain-like, F5/8C: Coagulation factor 5/8 domain. NCBI accession numbers for each protein are listed in Table S3.



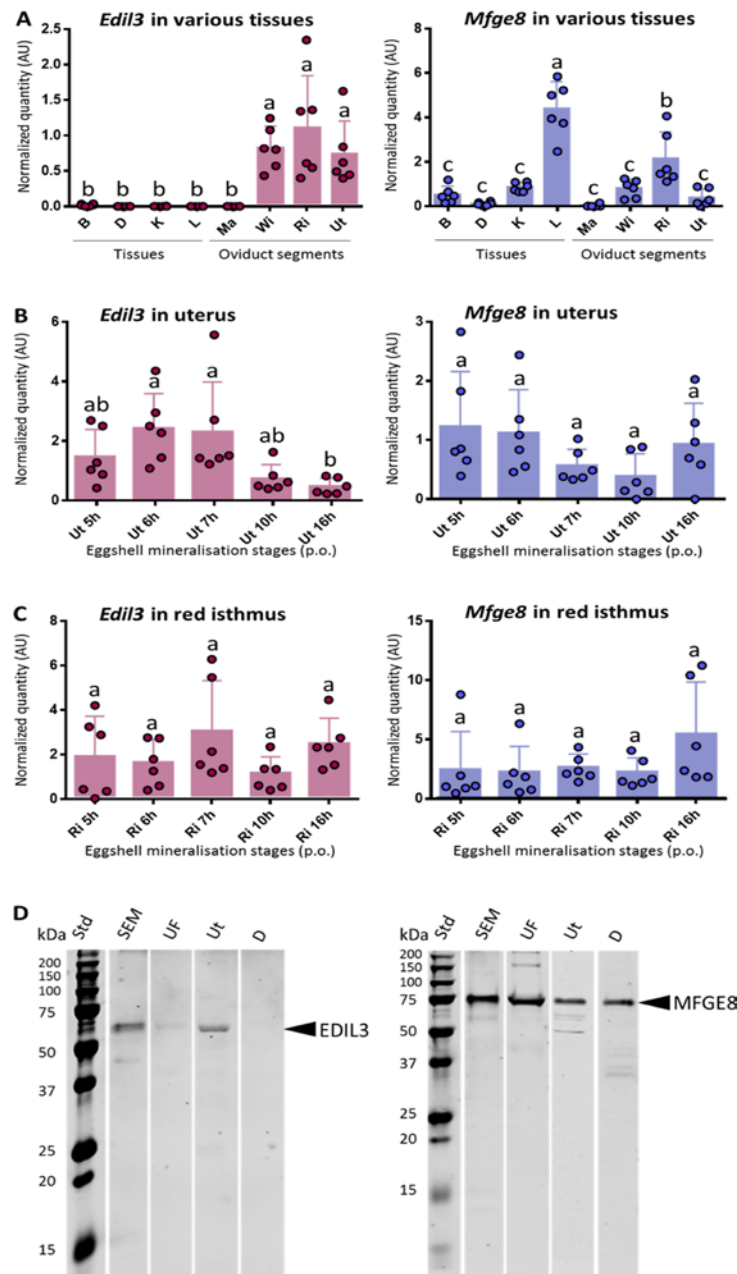


**Figure 3.** (A-C) Gene expression of *edil3* and *mfge8* in oviduct regions and four tissues of *Gallus gallus* at key events of eggshell biomineralisation. Each tissue and stage were determined on six different laying hens (n= 6) (A) *Edil3* and *mfge8* expression in oviduct regions and four tissues of *Gallus gallus*. All tissues were harvested at 10 h post-ovulation from 40-week hens, except for tibial bone (B), which is from 18 h post-ovulation in 90-week hens. (B) *Edil3* and *mfge8* expression in uterus at five key stages of eggshell biomineralisation (5 h, 6 h, 7 h, 10 h and 16 h post-ovulation). (C) *Edil3* and *mfge8* expression in red isthmus at five key stages of eggshell biomineralisation (5 h, 6 h, 7 h, 10 h and 16 h post-ovulation). Relative expression levels of genes were normalised with eight housekeeping genes (methods). Error bars indicate standard deviations. Different letters indicate significant differences in levels of expression (p-value<0.05), based on one-way Anova and pairwise Tukey test. B: Tibial bone, D: Duodenum, K: Kidney, L: Liver, Ma: Magnum, WI: White isthmus, RI: Red isthmus and Ut: Uterus. (D) Western blot analysis of EDIL3 and MFGE8 levels in soluble eggshell matrix (SEM), uterine fluid (UF), uterus (Ut) and duodenum (D). For each sample, 15  $\mu$ g of protein was subjected to electrophoretic separation and electro-transfer. The membranes were probed with anti-EDIL3 (left) or anti-MFGE8 (right) antibodies. AlexaFluor® 680 – labelled secondary antibody was used for the detection. Std: molecular mass standard.

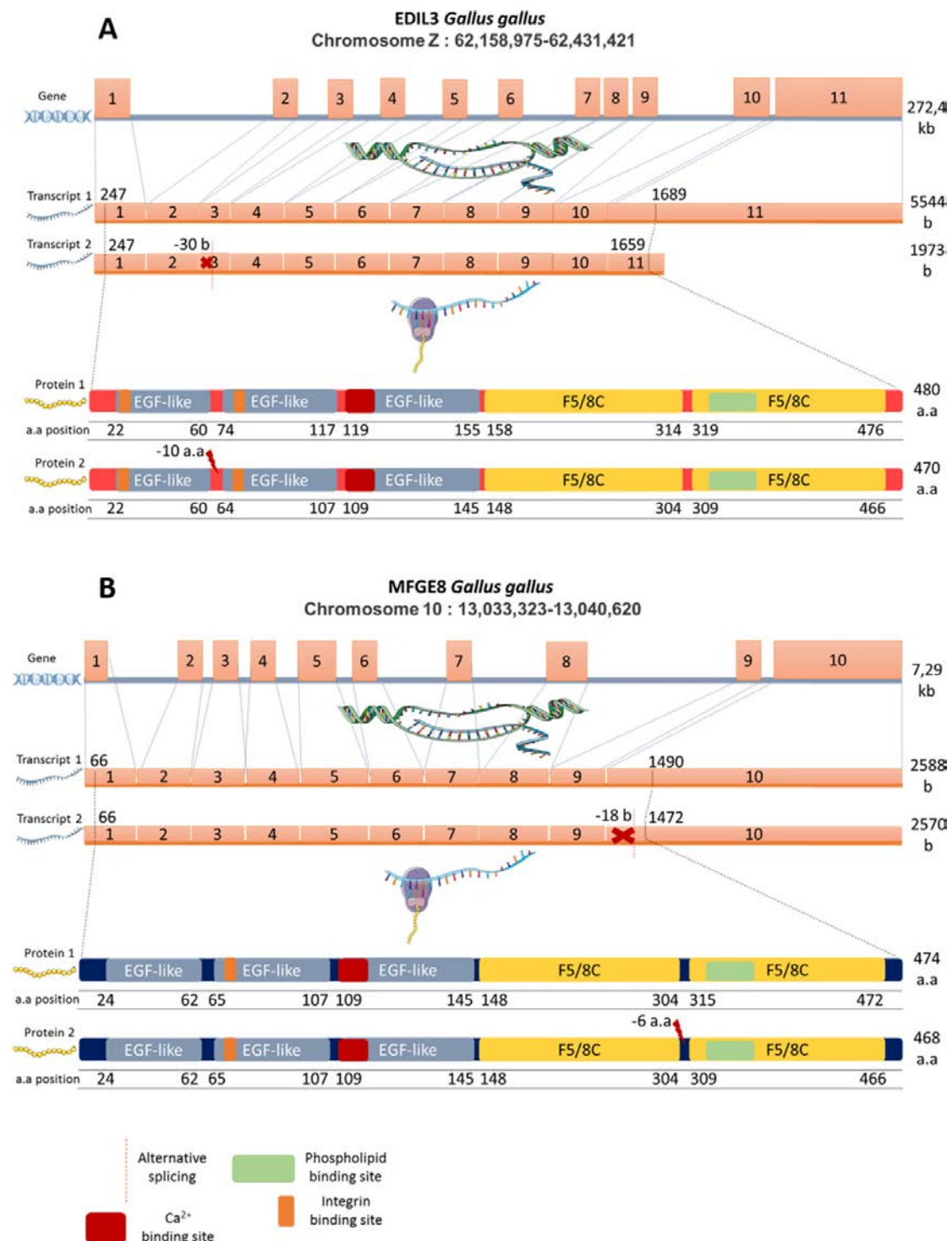


**Figure 4.** Gene, mRNA variants and protein isoforms for *Gallus gallus* (A) EDIL3 and (B) MFGE8. EGF: Epidermal growth factor-like domain, F5/8C: Coagulation factor 5/8 domain. The domain positions and sequence lengths were determined using the NCBI database. *Edil3* Gene ID: 427326; transcript 1, XM\_424906.6; transcript 2, XM\_004949448.3; protein isoform 1, XP\_424906.3; protein isoform 2, XP\_004949505.1. *Mfge8* Gene ID: 415494; transcript 1, NM\_001277110.1; transcript 2, NM\_001277111.1; protein isoform 1, NP\_001264039.1; protein isoform 2, NP\_001264040.1. Elements from Servier Medical Art (<https://smart.servier.com/>), licensed under a Creative Commons Attribution 3.0 Unported License.

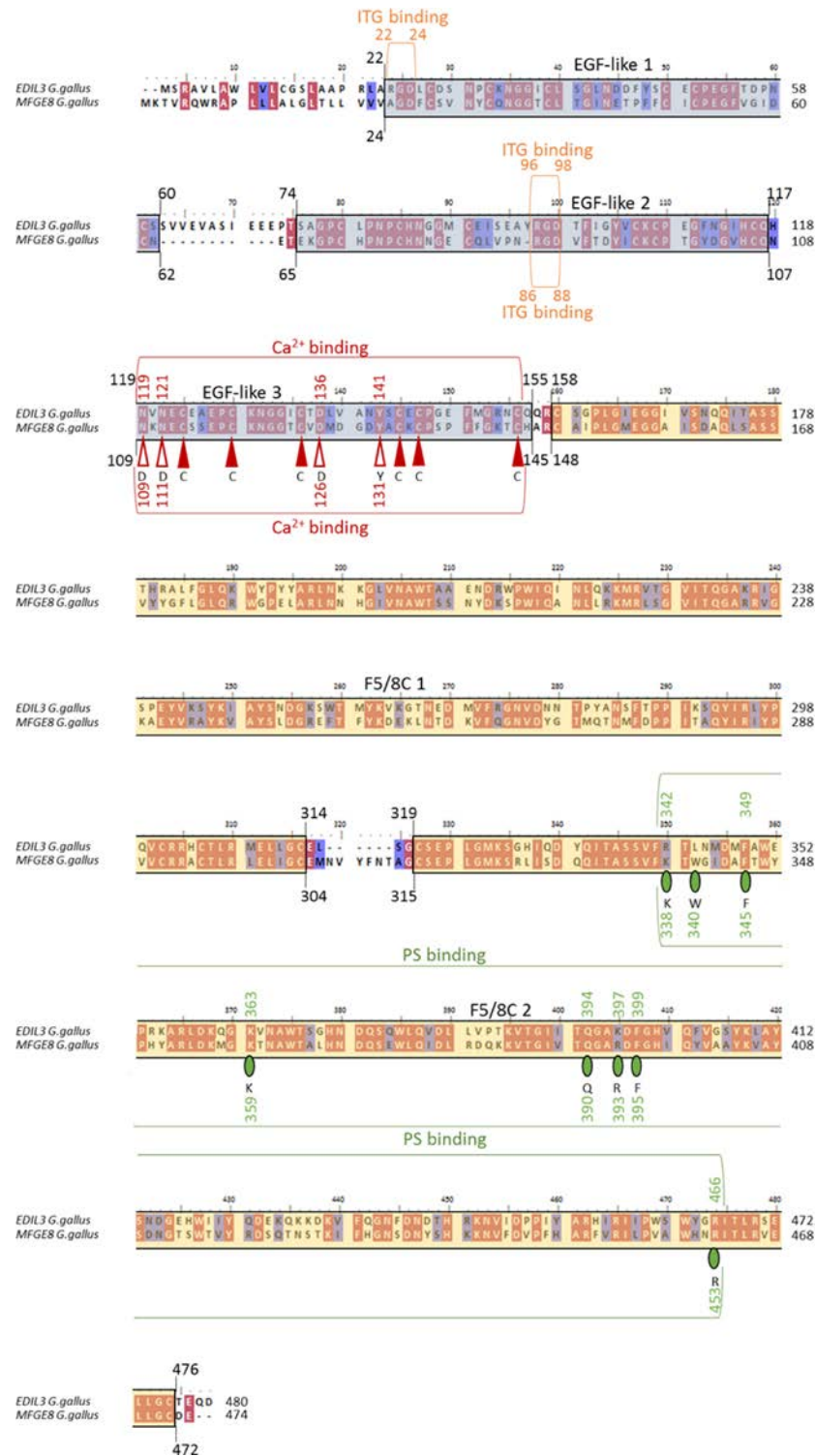


**Figure 5.** Domain prediction for *Gallus gallus* EDIL3 and MFGE8 protein sequences. GenBank accession numbers: EDIL3 XP424906.3; MFGE8 NP\_001264039.1. Alignment was performed using clustalΩ method in MEGA7 and then annotated with BioEdit. Red and blue coloured residues indicate identity and similarity, respectively. Blue and yellow backgrounds correspond to EGF-like and F5/8C domains, respectively. Red vertical arrows (filled for cysteines) and green circles correspond to amino acid residues involved in Ca<sup>2+</sup>-binding and phosphatidylserine (PS)-binding, respectively. The letters below the arrows and circles indicate the consensus pattern for Ca<sup>2+</sup>-binding and PS-binding residues of human coagulation factors IX/X and mouse MFGE8, respectively. Indicated positions correspond to the residue numbering for the full length sequences of *Gallus gallus* EDIL3 and MFGE8.

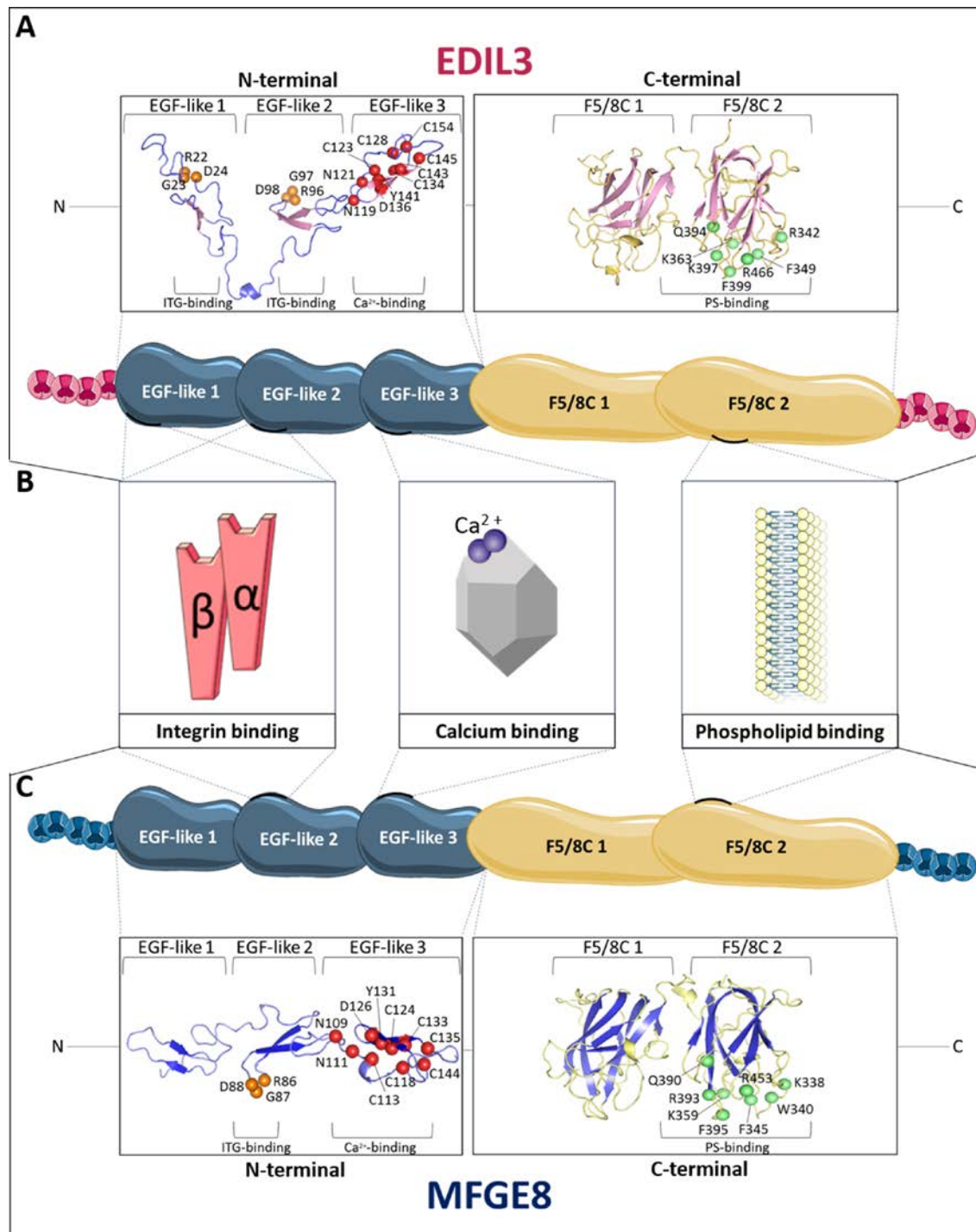


**Figure 6.** *In silico* prediction and structure modelling of EDIL3 and MFGE8 protein domains and binding sites. (A) Tertiary structure prediction of EGF-like and F5/8C regions of *Gallus gallus* EDIL3 (XP\_424906.3). (B) Schematic representation of *Gallus gallus* EDIL3 and MFGE8 protein domains including their binding sites. (C) Tertiary structure prediction of EGF-like and F5/8C regions of *Gallus gallus* MFGE8 (NP\_001264039.1). The tertiary structure prediction models were generated by EGF-like and F5/8C domain regions splitting using the I-TASSER template-based modelling. Following prediction modelling, the generated tertiary structures were edited using PyMOL. Orange balls indicate RGD residues of the ITG-binding sites, red balls illustrate residues of the Ca<sup>2+</sup>-binding sites and green balls display PS-binding sites. The position of the residues is indicated according to their location in the entire protein. ITG: Integrin, PS: Phosphatidylserine, EGF-like: Epidermal growth factor-like domain, F5/8C: Coagulation factor 5/8 domain. Elements from Servier Medical Art (<https://smart.servier.com/>), licensed under a Creative Commons Attribution 3.0 Unported License.



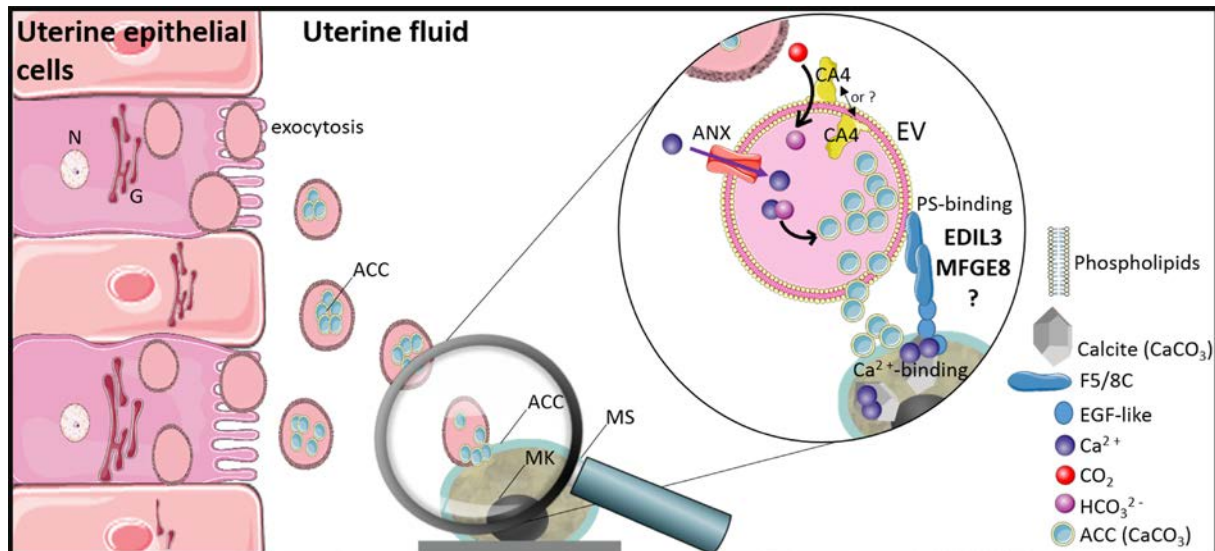


**Figure 7.** Schematic representation of proposed vesicular transport during eggshell mineralisation. Extracellular vesicles (EV) originate from the plasma membrane of the uterine epithelial cells and accumulate in the UF. Annexins (ANX) and carbonic anhydrase 4 (CA4) provide  $\text{Ca}^{2+}$  and  $\text{HCO}_3^-$  ions respectively for the accumulation of amorphous calcium carbonate (ACC) inside the EV. This mechanism implies ACC stabilisation by additional proteins. EDIL3 and MFGE8 are present at the EV surface due to their phosphatidylserine (PS)-binding motif. EVs target the mineralisation site (MS) through  $\text{Ca}^{2+}$ -binding of EDIL3 / MFGE8 and deliver the ACC required for mineral formation. MK: Mammary knobs. N: Nucleus, G: Golgi. Elements from Servier Medical Art (<https://smart.servier.com/>), licensed under a Creative Commons Attribution 3.0 Unported License.

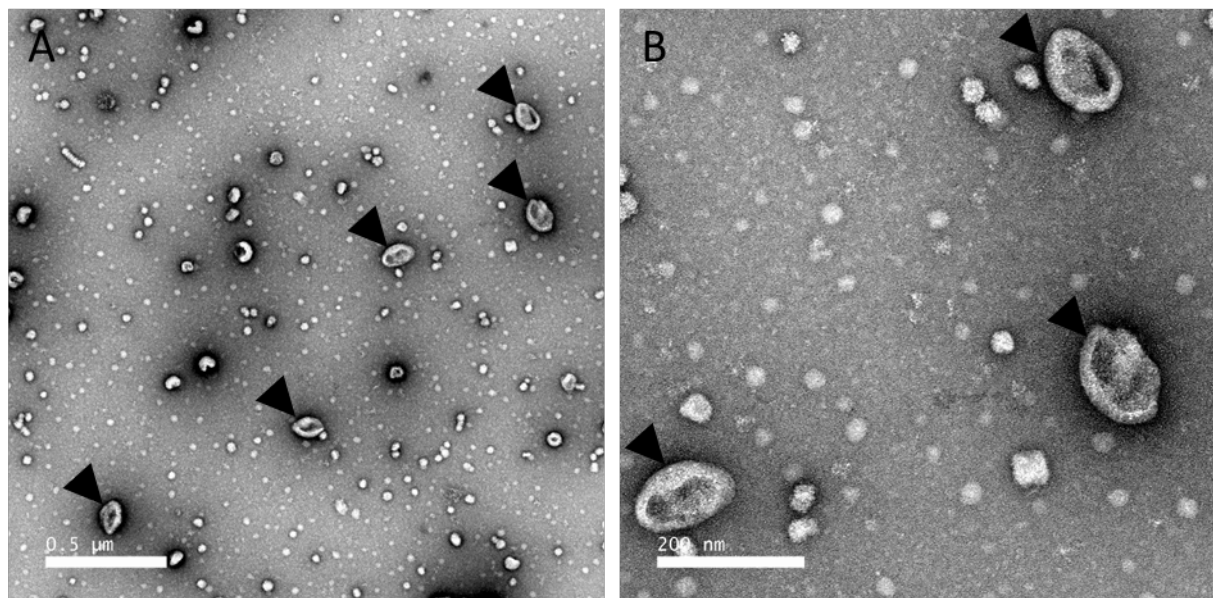


**Figure 8.** Transmission electron microscopy of extracellular vesicles (EV) fraction purified from uterine fluid harvested at 7 h post-ovulation. (A) Low magnification view; (B) Higher magnification TEM micrograph of the EVs. EVs were negatively stained with 2 % uranyl acetate (methods). Black arrowheads indicate extracellular EVs. Scale bars: A= 0.5  $\mu\text{m}$  and B= 200 nm.

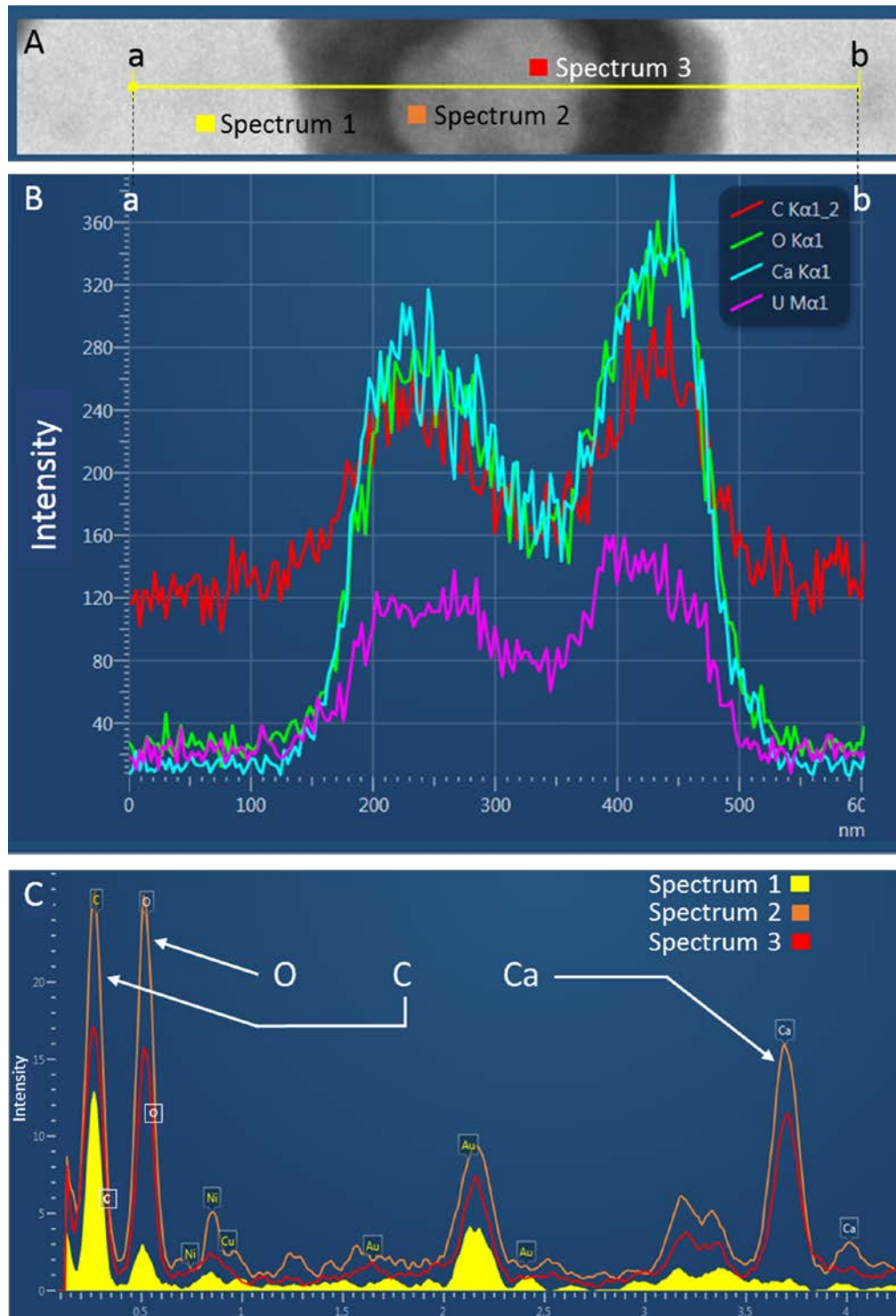


**Figure 9.** Transmission electron microscopy (TEM) and energy dispersive X-ray Spectroscopy analysis (EDS) on extracellular vesicle (EV) from uterine fluid (UF) collected at 16 h post-ovulation (p.o.).

(A) Transmission electron microphotography of an extracellular vesicle observed in uterine fluid. The yellow line (from points a to b) indicates the mapping zone across which EDS analysis was performed to obtain (B) the elemental spectra along the line for the indicated elements. (C) Spectrum 1 corresponds to EDS analysis of background in the absence of vesicles, whereas spectrum 2 and spectrum 3 correspond to EDS analysis at two different locations within a vesicle, as indicated in A. UF were negatively stained with uranyl acetate 2 %. Intensities are given in arbitrary units.